Small-Angle X-Ray Scattering Studies on Inhomogeneity in Aqueous Mixtures

The Thesis

for

the Degree of Doctor of Science

Submitted to

the Graduate University for Advanced Studies

by

Hisashi Hayashi

1991

Contents

Chapter 1

General Introduction

A concept of inhomogeneity is crucial in understanding properties of condensed matters.[1] Numerous studies concerning inhomogeneity have been made for various systems, such as colloidal solutions, colloidal powders, natural and synthetic high polymers, alloys, glasses, and so on.[1,2]

Aqueous mixtures often show anomalous behavior in various transport and thermal properties,[3] and formation of some kind of molecular aggregates or (micro)inhomogeneity has generally been invoked for explaining these peculiarities. Studies on inhomogeneity of the mixtures are, however, few and accordingly details are not clear as yet. Inhomogeneity in aqueous mixtures is also a clue to monitoring progress of some chemical reactions such as polymerization. Studies along this line are also scarce.

In this thesis, the author has tried to examine static as well as dynamic inhomogeneity in several aqueous mixtures by using the small angle X-ray scattering (SAXS) method. The SAXS method has been one of the most direct methods to investigate inhomogeneity in condensed matters since early 1930's.[4,5]

Accurate SAXS data must be collected in a short period of time for the present purposes. Traditional SAXS diffractometers with line-focusing optics are inadequate to obtain accurate data because of errors due to the collimation effect. A new SAXS diffractometer was accordingly constructed by employing a point-focusing optics with a double-bent monochromator. The diffractometer has been tested for several pure liquids and aqueous solutions. It was found that the diffractometer can

supply intense enough incident beams and minimize errors due to the collimation effect. The design and performance of the diffractometer are described in detail in Chapter 2, as well as analytical procedures of SAXS data obtained.

The use of the diffractometer has opened up two new possibilities: thorough understanding of static inhomogeneity and pursuit of dynamic inhomogeneity.

Improvement in accuracy of the SAXS data by using the diffractometer has made it possible to extract a new parameter about inhomogeneity. For an isotropic sample such as aqueous organic solutions, SAXS intensity curves (I(s)) can be approximated by a polynomial for small scattering angles.[2] The parameters used in previous SAXS studies for aqueous organic solutions, such as concentration fluctuation[6] and correlation length,[1,7] are related to coefficients of the 1st and 2nd terms in the polynomial. Now the coefficient of the 3rd term can be accurately obtained and a new parameter χ, derived from coefficients of the 1st, 2nd, and 3rd terms in the polynomial, is proposed. The physical meaning of χ is discussed in Chapter 3.

SAXS data for aqueous organic solutions of 2-butoxyethanol (BE) and 1-propanol (NPA) are analyzed in Chapters 4 and 5, respectively. BE aqueous solution has a lower critical solution temperature (LCST) near room temperature,[8,9] and its correlation length showed very large variations with temperature and concentration. On the contrary, NPA aqueous solution has no critical temperature (i.e., NPA mixes with water at any

temperature and concentration), and its correlation length showed slight variations with concentration and almost no temperature dependence. Thus the mixing states of the two systems are markedly different; local structure in BE/NPA aqueous solutions changes drastically/modestly with temperature and concentration. The difference is sensitively reflected to χ. In terms of the obtained χ's, new aspects of mixing states of BE and NPA aqueous solutions are discussed in Chapters 4 and 5, respectively.

In Chapter 6, dynamic inhomogeneity has been studied for several aqueous mixtures composed of metal ethylene glycolates and tetraethoxysilane. In the systems studied, metal silicates slowly grow, eventually forming gels.[10] The change of I(s) with time, due to the growth of the metal silicates, was evaluated through Guinier radius[2] and Porod slope.[11,12] Time dependence of these parameters has shed some light on the mechanism of the growth of the silicates or the dynamic inhomogeneity.

References

1. J. M. Ziman, "Models of Disorder," Cambridge University Press, Cambridge (1979).
2. G. Porod, "Small Angle X-ray Scattering," ed O. Glatter and O. Kratky, Academic Press, London, p.17 (1982).
3. Y. Marcus, "Introduction to Liquid State Chemistry," John Wiley & Sons, New York (1977).
4. H. Mark, "Physik und Chemie der Zellulose," Springer (1932).
5. S. B. Hendricks, Z. Krist. Mineral Petrog., **83A**, 503 (1932).
6. A. B. Bhatia and D. E. Thornton, Phys. Rev., B **2**, 3004 (1970).
7. P. Debye, J. Chem. Phys., **31**, 680 (1959).
8. N. Ito, T. Fujiyama, and Y. Udagawa, Bull. Chem. Soc. Jpn., **56**, 379 (1983).
9. C. Baaken, L. Belkoura, S. Fusenig, Th. Müller-Kirschbaum, and D. Woermann, Ber. Bunsenges. Phys. Chem., **94**, 150 (1990).
10. A. Ueno, H. Suzuki, and Y. Kotera, J. Chem. Soc. Faraday Trans., **79**, 127 (1983).
11. D. W. Schaefer, Science, **243**, 1023 (1989).
12. D. W. Schaefer and K. D. Keefer, Phys. Rev. Lett., **53**, 1383 (1984).

Chapter 2

Construction of a Point-Focusing SAXS Diffractometer

2.1 Introduction

The small-angle X-ray scattering (SAXS) method is one of the most direct ways to obtain information on the structure of inhomogeneities in a system. A variety of SAXS diffractometers or cameras have been developed for various purposes, each having its own advantage with respect to resolution and intensity.

In studies of solutions composed of molecules with low molecular weight, SAXS provides various measures concerning microinhomogeneities in liquids, such as concentration fluctuation,[1] the Kirkwood-Buff parameters,[2] and Debye's correlation length.[3] Inherently weak SAXS intensities from those solutions require an intense incident beam. Line-focusing diffractometers therefore have been used in this field: Kratky cameras,[4-6] diffractometers with a single bent LiF monochromator[7,8] and those with a focusing bent mirror.[9,10]

Although relatively weak in intensity, point-focusing diffractometers are more advantageous to obtain accurate SAXS data due to the collimation effect. For conventional X-ray sources, a diffractometer with a double-bent LiF crystal monochromator[11,12] may be the only point-focusing one to provide sufficiently intense incident beams to measure SAXS on molecular solutions. The difficulty of preparing the double-bent crystal, however, has prevented the general use of this optics so far. Now, this difficulty has been alleviated by the development of computer-controlled milling machines by which toroidal convex and concave molds can be easily made. Thus, the author has

constructed a point-focusing diffractometer with a double-bent LiF crystal monochromator and has measured SAXS on molecular solutions by using point-focusing optics for the first time.

In this chapter, the author describes the design of the diffractometer, and reports SAXS measurements for several pure liquids and aqueous solutions to evaluate the performance of the diffractometer as well as the analytical procedures of SAXS data.

2.2 General Layout of the Diffractometer

A schematic representation of the diffractometer is given in Fig. 2-1. It consists of an X-ray source, an ionization chamber, two X-Y apertures, a double-bent LiF (200) crystal, a cell holder, a beam stopper, a vacuum chamber, and a detector.

A rotating-anode generator (RU-200, Rigaku Denki) with a Cu target was employed. The generator was operated at 50 kV and 180 mA. The intensity of white X-rays was monitored by an ionization chamber placed at the opposite side of the monochromator, and the fluctuation of X-rays was corrected by assuming that the spectral distribution remained constant.

The radius of curvature of the double-bent LiF crystal in the horizontal plane R_1 is 1830 mm and that in the vertical plane R_2 is 378 mm. The crystal was made of a cleft LiF (200) single crystal with a size of 50 mm * 40 mm * 2 mm. Details are as follows: The LiF crystal was sandwiched between toroidal convex and concave molds. Then it was heated in a silicon-oil bath up to 250 °C, pressed gradually and annealed for 8 h. The molds were made of aluminum metal and the toroidal surfaces were formed

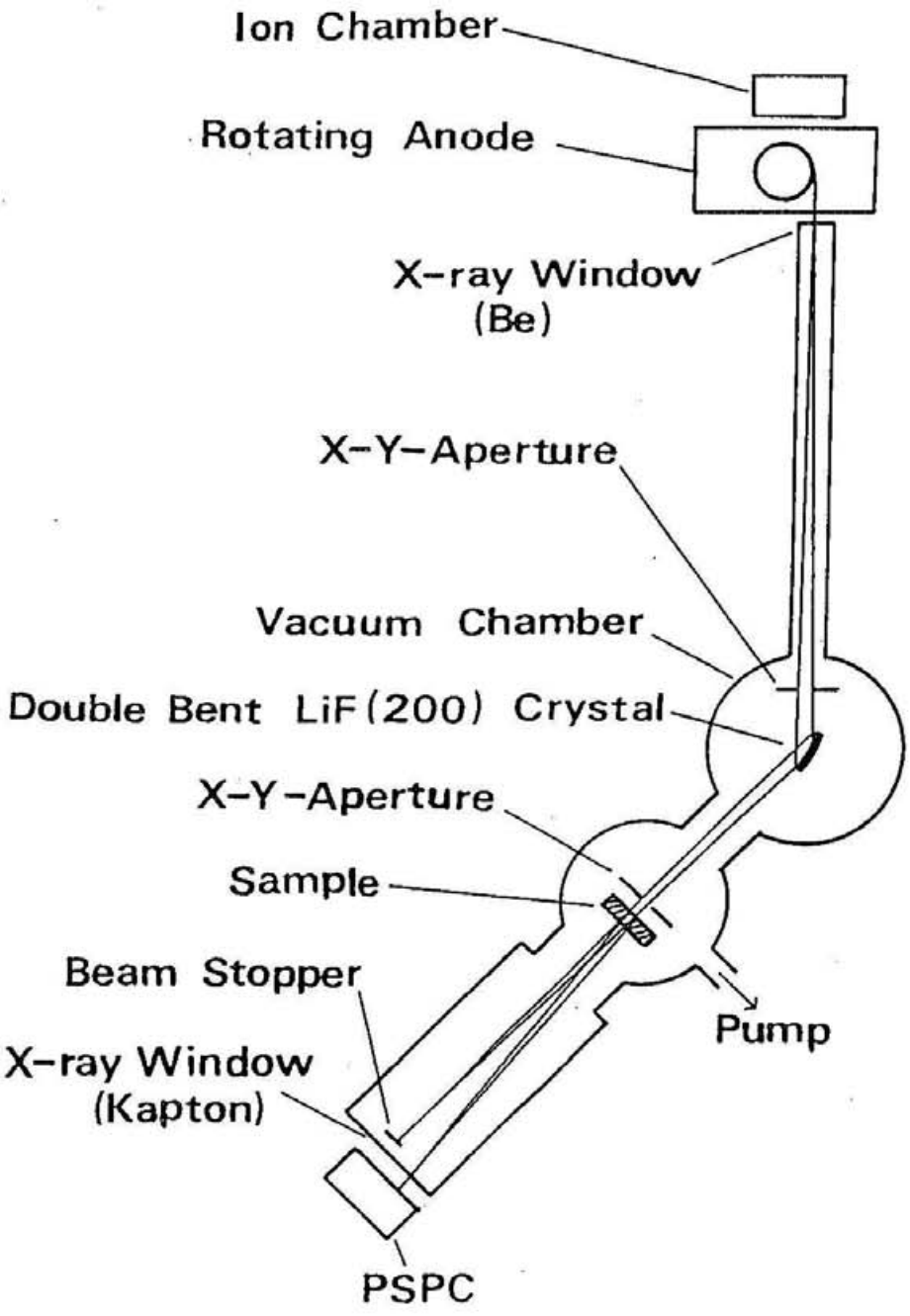

Figure 2-1. A schematic representation of the point-focusing SAXS diffractometer.

by using a computer-controlled milling machine. The radii of curvature of the double-bent crystal determine the focal length, which is the distance between the monochromator and the detector, to be 700 mm for Cu Kα radiation. The camera length, which is the distance between the sample and the detector, was chosen to be 415 mm as a compromise between the intensity and the small-angle resolution.

To ascertain the uniformity of the bent crystal, the shape of the monochromatized beam was photographed at various positions. The primary white X-rays have a focal size of 1 mm * 1 mm. The cross section of the X-ray beam is about 5 mm * 5 mm near the crystal surface. Images of the beam shown in Fig. 2-2 indicate the uniformity of the crystal.

To remove any parasitic scattering from the crystal, two X-Y apertures are set: one before the crystal and the other close to the cell holder. The apertures are made of 1 mm-thick tantalum blocks which are movable independently in the horizontal direction. In the SAXS measurement, the aperture before the crystal was adjusted to 10 mm (vertical) * 1.5 mm (horizontal) and the one close to the cell holder was adjusted to 5 mm (vertical) * 0.8 mm (horizontal). In this setting, the irradiated area on the sample is 2.8 mm (vertical) * 0.8 mm (horizontal), and the diffractometer can cover scattering angles ranging from 0.42° to 5.62°. The range corresponds to s = 0.03 - 0.40 $\mathring{A}^{-1}$ for Cu Kα radiation. Here, s is the scattering parameter defined by $s = 4\pi \sin\theta / \lambda$, where 2θ is the scattering

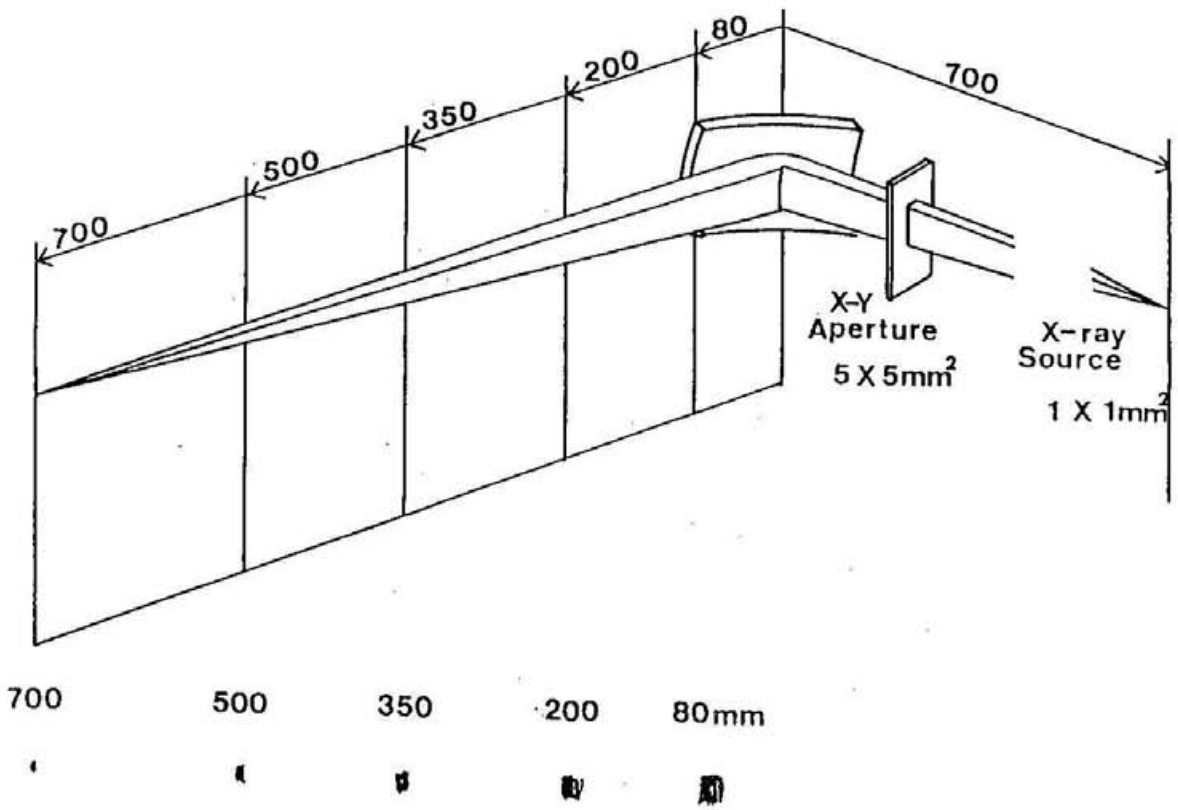

Figure 2-2. Pictures of the focused X-ray beam taken at different distances from the double-bent LiF crystal.

angle and λ is the wavelength of X-rays. Although the small-angle resolution of this diffractometer is inferior to those of high-resolution SAXS diffractometers for the study of polymers ($s > 0.002$ $\mathring{A}^{-1}$ [13] or $s > 0.00014$ $\mathring{A}^{-1}$ [14]), it is sufficient for SAXS measurements of solutions composed of molecules with low molecular weights. Indeed, the resolution is comparable to or even better than those of other line-focusing SAXS diffractometers employed in previous studies on molecular solutions ($s > 0.025$ $\mathring{A}^{-1}$,[15] 0.03 $\mathring{A}^{-1}$,[4,6,8] 0.05 $\mathring{A}^{-1}$,[10] 0.07 $\mathring{A}^{-1}$,[9] and 0.15 $\mathring{A}^{-1}$ [7]).

The cell holder made of Cu is coupled to a bath circulator, with which the temperature of a sample is variable from ca. -5 to 70 °C and can be kept constant within 0.5 °C. The sample cell with a ϕ 10 mm-window is also made of Cu. To avoid erosion, the cell was coated with gold and the O-rings "Kalretz" (Dupont), which show excellent corrosion resistance, were adopted as packing material. Two 0.1 mm-thick mica films were employed as window material. The films were superior to the Al sheets in regard to corrosion resistance, tolerance to vacuum, and transmittance of X-rays. The tolerance to vacuum is especially important. In the cell with the Al windows, leak started after several measurements, but no leak was observed in the cell with the mica windows, even after repeating 50 measurements. Moreover, the distortion of the windows under a reduced pressure in the X-ray path, which causes large errors in the correction of background scattering, was smaller in the cell with the mica

windows than in that with the Al windows.

Unfortunately, mica gives stronger background scattering than Al; the intensity of background scattering in the small angle from 0.1 mm-thick mica films was over 1.5 times than that from the 25 μm-thick Al sheets previously used,[15] although it was 1/10 of that from the 0.2 mm-thick Be windows and 1/3 of that from the 25 μm-thick Mylar windows. The influence of the background scattering, however, can be corrected as shown in the section 2.4.

The double-bent LiF crystal, the cell holder, two X-Y apertures and the beam stopper are placed in a vacuum chamber in order to reduce scattering by air.

The author adopted a PSPC probe (PSPC5, Rigaku Denki) and a position analyzer system as a detector. Details of this system are the same as those reported previously,[15] except for the use of a 35 plus (Canberra) multichannel analyzer.

2.3 SAXS Measurements of Solutions

The SAXS spectra on water, methanol, and 1-propanol (abbreviated to NPA) were measured at 25 °C to ensure the performance of the diffractometer as well as the validity of the analytical procedures. The SAXS spectra on the following aqueous solutions, which are known to show a large collimation effect, were also measured to ascertain the improvement by using the point-focusing optics: an NPA aqueous solution (C_1= 0.20, C_1: the mole fraction of alcohol) at 25 °C and a t-butyl alcohol (TBA) aqueous solution (C_1= 0.20) at 25 and 40 °C.

Water was deionized and distilled. Organic chemicals of reagent grade with a 99.9% purity were used after drying by molecular sieves (3A 1/8, Aldrich). Aqueous solutions were prepared by weighing the components.

The count rate of SAXS signals from water, the SAXS intensity of which is very weak, was 0.12 count/(s.channel). The rate is about 5 times as large as that obtained by a line-focusing diffractometer combined with a 0.9 kW X-ray generator, which has been used in previous works.[15] The result shows that the beam intensity on the present diffractometer is intense enough to measure SAXS on solutions composed of molecules with low molecular weight; in an accumulation time of 10000 - 20000 s, the total count number per channel amounts to typically 5000 - 20000 counts.

In addition to the increased intensity, the cross section of the X-ray beam on the sample is also reduced. It is 2.24 mm^2 and is about 1/6 of that of the previous diffractometer, indicating that the collimation effect can be minimal. The extent of the collimation effect will be discussed in detail later.

2.4 Analytical Procedures

2.4.1 Correction of background scattering and conversion into absolute scale

All SAXS data were treated as follows: The measured intensities were collected in terms of the count rate of scattered X-rays from the sample (I_s) as a function of s in the range of 0.03 to 0.40 $\mathring{A}^{-1}$. The I_s includes intensities of

scattered X-rays by the cell windows (I_b) and the dark count (I_d). I_b and I_d were determined by measurements with the empty cell and with X-rays off, respectively. The correction for the background scattering and the conversion of the measured intensities into absolute scale can be performed by the following equation:

$$I_1(s) = Z \cdot P\{(I_s(s)-I_d(s)) - (I_b(s)-I_d(s)) \cdot \exp(-\mu_s t_s)\} / \exp(-\mu_s t_s - \mu_b t_b), \quad (2\text{-}1)$$

where μ_s and μ_b are the linear absorption coefficients of the sample and the windows, respectively, t_s and t_b are the thickness of the sample and the windows, respectively, and P is the conversion coefficient. Z is the factor which corrects for intensity fluctuation of the primary beam and is defined as $Z = I_{0b}/I_{0s}$. Here, I_{0s} and I_{0b} are the average intensities of the primary beam in measurements of the scattering from a sample and an empty cell, respectively. The product $\mu_b t_b$ was determined from intensity measurements by an ionization chamber with and without the cell. The value of μ_s was calculated by using atomic mass absorption coefficients tabulated in the International Tables.[16]

A precise t_s-value is required in the analysis of SAXS, especially in the case of intense background scattering. The t_s-value determined by a simple measurement of the attenuation of the beam was, however, found not to be sufficiently precise, probably due to the distortion of windows. The values, t_s and P,

were accordingly determined by the least-squares method as follows: The absolute scattering intensity from the ideal pinhole collimation extrapolated to s = 0 (I(0)) on a pure liquid is linked to thermodynamic parameters by the Ornstein-Zernike equation:[17]

$$I(0) = Z_e^2 N^2 \kappa_T k_B T/V, \qquad (2\text{-}2)$$

where κ_T is the isothermal compressibility of the liquid, Z_e is the number of electrons in a molecule of the liquid, N is the number of molecules in the volume V, k_B is the Boltzmann constant and T is the absolute temperature. The I(0) values of three pure liquids (water, methanol and NPA) were calculated from eq. (2-2) by employing the literature values of κ_T[18-22] and density data.[23,24] The I(0) values were experimentally determined after the correction as described in the section 2.4.2. Then, the values of t_s and P of 0.245 cm and 1.57, respectively, were obtained by the least-squares calculation.

2.4.2 Correction of the collimation effect

A measured SAXS intensity curve ($I_1(s)$) includes contributions of Compton scattering and multiple scattering. They were estimated theoretically[25] and the experimental SAXS intensity curve ($I_2(s)$) was obtained after subtraction of the contributions.

The $I_2(s)$ should be further corrected for the collimation effect and the wavelength effect. The former comes from a finite spot size and the latter is caused by overlapping of the Cu $K\alpha_1$

and $K\alpha_2$ lines in the beam of the present diffractometer.

The SAXS intensity curve on solutions composed of molecules with low molecular weight usually varies slowly, and therefore it is reasonable to analyze the SAXS data of the solutions by a polynomial function of s^2, as has been done by Walter and Schmidt.[26] The author approximated that each $I_2(s)$ in the range $0.03 \leq s \leq 0.21$ $\overset{\circ}{A}^{-1}$ can be expressed as follows:

$$I_2(s) = a + bs^2 + cs^4 + ds^6. \qquad (2\text{-}3)$$

The coefficients (a, b, c, and d) were determined by the least-squares calculation, and the R-factor defined in eq. (2-4) did not exceed 0.0001 in all of the measurements:

$$R = \Sigma (I_2^{obs} - I_2^{cal})^2 / \Sigma (I_2^{obs})^2, \qquad (2\text{-}4)$$

where I_2^{obs} is the measured intensity corrected for the terms as described in 2.4.1 and I_2^{cal} is the intensity calculated by eq. (2-3). The SAXS intensity curve from the ideal pinhole collimation (I(s)) is also an even function of the 6-th order:

$$I(s) = A + Bs^2 + Cs^4 + Ds^6. \qquad (2\text{-}5)$$

This derivation is so complicated that it will be shown in another section (2.4.3). The coefficients in eq. (2-5) are related to those of eq. (2-3) as shown in eqs. (2-6) through (2-10). The relations will also be discussed in the section 2.4.3.

$$D = d/G_3, \tag{2-6}$$

$$C = (c - 3KG_3D(5w^2 + h^2))/G_2, \tag{2-7}$$

$$B = (b - 2KG_2C(3w^2 + h^2))/G_1, \tag{2-8}$$

$$A = a - KG_1B(w^2 + h^2), \tag{2-9}$$

$$K = 4\pi^2/(3\lambda_0^2L^2), \tag{2-10}$$

where w and h are the half-widths on the irradiated plane in the horizontal direction and the vertical direction, respectively, L is the camera length, λ_0 is 1.5405 Å (Cu Kα_1), and G_1= 0.9984, G_2= 0.9967, and G_3= 0.9951. Equations (2-6) - (2-10) are an extension of Walter and Schmidt's equations,[26] and include the collimation effect in the horizontal plane and the wavelength effect. By eqs. (2-6) - (2-10), the collimation effect and wavelength effect can be corrected.

2.4.3 Derivation of eqs. (2-6) - (2-9)

The slit-smeared SAXS intensity curve ($I_2(s)$) is related to the SAXS intensity curve from the ideal pinhole collimation I(s) as follows (see Fig. 2-3):[27]

$$I_2(s) = \iiint p(x)q(y)w(\lambda')I(2\pi((m-x)^2+y^2)^{0.5}/(\lambda'L))dxdyd\lambda', \tag{2-11}$$

where p(x) and q(y) are the weight functions for the X-ray intensity on the irradiated plane of a sample in the horizontal direction x and the vertical direction y, respectively, and $w(\lambda')$ is the weight function for the wavelength λ' of the monochromatized beam. Here, m is the distance between the scattered beam and the center of the monochromatized incident

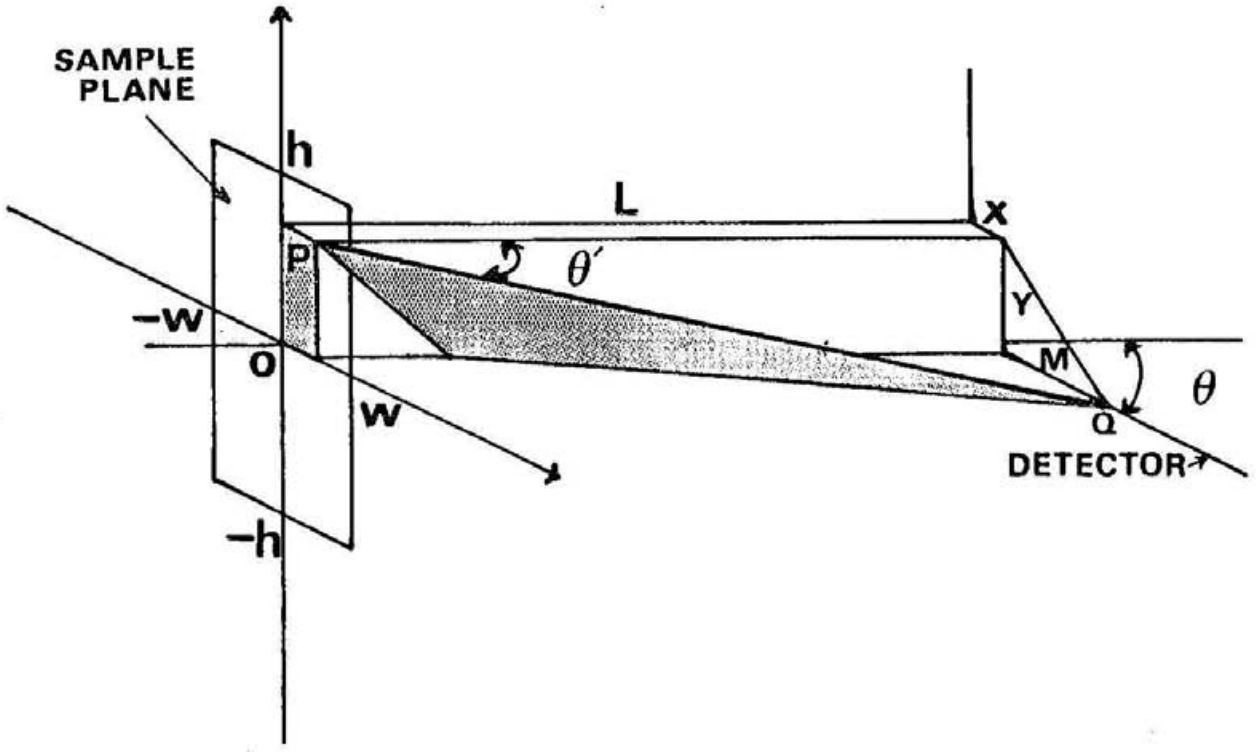

Figure 2-3. Geometrical description of the collimation effect.

beam on the detector plane.

Strictly speaking, eq. (2-11) holds only for parallel incident beams, and the effect caused by beam divergence must be taken into consideration under the experimental condition employed here. The error due to the effect is, however, estimated to be about 1/3 of that due to the collimation effect and is accordingly neglected.

In order to derive eqs. (2-6) - (2-9), the I(s) approximated by eq. (2-5) is substituted into eq. (2-11) under the setting of the weight functions as follows:

$$p(x)=\begin{cases} 1/(2w) & (-w \leq x \leq w) \\ 0 & \text{otherwise,} \end{cases} \tag{2-12}$$

$$q(y)=\begin{cases} 1/(2h) & (-h \leq y \leq h) \\ 0 & \text{otherwise,} \end{cases} \tag{2-13}$$

$$w(\lambda')= (2/3)\cdot\delta(\lambda'-1.5405) + (1/3)\cdot\delta(\lambda'-1.5443). \tag{2-14}$$

Here, the above setting of p(x) and q(y) (eqs. (2-12) and (2-13)) and that of $w(\lambda')$ (eq. (2-14)) correspond to the approximation that the incident beam is perfectly parallel and uniform on the irradiated plane[25] and that only Cu $K\alpha_1$ and $K\alpha_2$ lines exist in the monochromatized incident beams in the ratio of 2 : 1, respectively. From eqs. (2-11) to (2-14), the following

equations are obtained:

$$I_2(s) = a + bs^2 + cs^4 + ds^6, \tag{2-3}$$

$$a = A + 4\pi^2 G_1 B(w^2 + h^2)/(3\lambda_0^2 L^2), \tag{2-15}$$

$$b = G_1 B + 8\pi^2 G_2 C(3w^2 + h^2)/(3\lambda_0^2 L^2), \tag{2-16}$$

$$c = G_2 C + 12\pi^2 G_3 D(5w^2 + h^2)/(3\lambda_0^2 L^2), \tag{2-17}$$

$$d = G_3 D. \tag{2-18}$$

The terms above the $1/L^4$-term were neglected in the derivation of eqs. (2-15) - (2-18). Equation (2-3) shows that the slit-smeared SAXS intensity curve, as well as the SAXS intensity curve from the ideal pinhole collimation, is expressed as an even function of the 6-th order.

Equations (2-6) - (2-9) can be obtained from eqs. (2-15) - (2-18).

2.4.4 Parameters obtained from SAXS

The zero-angle scattering intensity[10] from the ideal pinhole collimation (I(0)) and Debye's correlation length[3] (L_D) are important measures for the microinhomogeneity in liquids. They can be obtained through the use of coefficients in eqs. (2-8) and (2-9) as follows:

$$I(0) = A, \tag{2-19}$$

$$L_D = (-6B/A)^{0.5}. \tag{2-20}$$

The I(0) values obtained for water, methanol, and NPA are tabulated in Table 2-1. For comparison, the I(0) values calculated by eq. (2-2) for these pure liquids are also tabulated

Table 2-1. Zero-angle scattering of pure substances at room temperature (25° C).

Sample	$I^{calc}(0)$ $/10^{23}$e.u.cm^{-3}	I(0) $/10^{23}$e.u.cm^{-3}
Water	2.09[a]	2.08
Methyl alcohol	3.62[b] - 3.70[c]	3.74
n-Propyl alcohol	3.07[d] - 3.13[e]	3.13

$I^{calc}(0)$ is the value calculated by means of the Ornstein-Zernike equation by using the literature values: a) cited from refs. 17 and 22, b) from refs. 18 and 23, c) from refs. 19 and 23, d) from refs. 20 and 23, and e) from refs. 21 and 23. I(0)'s are the experimental values.

in Table 2-1. The B value of the pure liquids is too small to determine L_D. The I(0) and L_D values of aqueous solutions are shown in Table 2-2 with the values before the correction of the collimation effect.

2.5 Discussion

The accuracy of the calculated values in Table 2-1 depends on the uncertainty of the thermodynamic values. Although differences among the literature values on V are less than 0.03 %, those of κ_T amount to as much as 2.5 - 3 %, which result in the change in the I(0) values calculated on methyl alcohol, for example, from 3.62 to 3.70 at different κ_T values. Thus, it can be concluded that the observed I(0) values agree well with the calculated ones within the uncertainty resulting from errors in thermodynamic data.

The collimation effect can be estimated from eqs. (2-6) - (2-9). Since a finite size of the X-ray beam causes errors due to the collimation effect, the errors are more significant for line-focusing optics than point-focusing one. It is also known that the collimation effect is large for the SAXS intensity curve with a steep slope.[26] The I(s) curve for a 20 mol% TBA aqueous solution is known to have the steepest slope among I(s) curves for the solutions with no critical point so far studied.

The collimation effect on I(0) in the TBA solution at 40 °C is significant in the line-focusing optics. The error due to the effect can be evaluated from the coefficients (A and B) obtained by the present measurement and eq. (2-9), and the error at w =

Table 2-2. Comparisons between the SAXS data on aqueous solutions before and after the correction of the collimation effect.

Sample	The SAXS data after the correction		The SAXS data before the correction	
	I(0) /10^{23}e.u.cm^{-3}	L_D /Å	I(0) /10^{23}e.u.cm^{-3}	L_D /Å
NPA 20% aq. solution at 25° C	16.31	12.5	16.28	12.5
TBA 20% aq. solution at 25° C	19.45	13.2	19.42	13.2
TBA 20% aq. solution at 40° C	24.42	14.3	24.38	14.3

0.5 mm amounts to 15 % for h = 20 mm, 9 % for h = 15 mm, and 4 % even for h = 10 mm. On the other hand, the error due to the collimation effect in the present point-focusing optics, shown in Table 2-2, is less than 0.2 %. The results for other solutions also show a negligible collimation effect. Hence, solutions with no critical point, whose I(s) curves are not so steep, can be studied without correction of the collimation effect. Even solutions with critical point may be studied after a minor correction, unless it is close to the critical point.

Since the possible errors caused by the finite beam size are minimal with the present diffractometer, the principal origin of errors must come from the background scattering. Water has the largest background scattering among the samples studied here. The signal/noise ratio on the SAXS intensity was 1.0 for water, 2.5 for lower alcohols, and 3 - 5 for alcohol aqueous solutions. Although no result is presented here, various organic liquids have been tested and found to give less background scattering than water. Thus, accurate SAXS data on molecular liquids can be obtained with the diffractometer described here.

2.6 Conclusions

A point-focusing diffractometer for measurements of SAXS from molecular solutions has been constructed. This diffractometer consists of a double-bent LiF monochromator whose focal length is 700 mm for Cu Kα radiation, a sample cell with 0.1 mm-thick mica windows, a bath circulator coupled with a cell holder, and a PSPC system. A small-angle resolution of better

than 0.42° is achieved with this diffractometer. To evaluate the applicability of the diffractometer, SAXS intensities on several pure liquids and aqueous solutions were measured. The results show that the diffractometer can produce incident beams intense enough to measure SAXS on the solutions and reduce errors arising from the collimation effect to a negligible amount.

References

1. A. B. Bhatia and D. E. Thornton, Phys. Rev., B **2**, 3004 (1970).
2. J. G. Kirkwood and F. P. Buff, J. Chem. Phys., **19**, 774 (1951).
3. P. Debye, J. Chem. Phys., **31**, 680 (1959).
4. Y. Koga, Chem. Phys. Lett., **111**, 176 (1984).
5. W. Kopp and J. H. Wendorff, Mol. Cryst. & Liq. Cryst., **84** 63 (1982).
6. Y. Izumi, Phys. Rev. A, **39**, 5826 (1989).
7. L. Bosio, J. Teixeira and H. E. Stanley, Phys. Rev. Lett., **46**, 597 (1981).
8. H. Hayashi, K. Nishikawa and T. Iijima, J. Phys. Chem., **94**, 8334 (1990).
9. K. Nishikawa, Y. Kodera and T. Iijima, J. Phys. Chem., **91**, 3694 (1987).
10. K. Nishikawa, H. Hayashi and T. Iijima, J. Phys. Chem., **93**, 6559 (1989).
11. N. Sakabe, J. Appl. Cryst., **16**, 542 (1983).
12. J. Witz, Acta. Cryst., **A25**, 30 (1969).
13. O. Yoda, J. Appl. Cryst., **17**, 337 (1984).
14. H. Hayashi, F. Hamada and S. Suehiro, J. Appl. Cryst., **21**, 330 (1988).
15. H. Hayashi, K. Nishikawa and T. Iijima, Jpn. J. Appl. Phys., **28**, 1501 (1989).

16. "International Tables for X-ray Crystallography," Kynoch Press, Birmingham (1968) Vol. III.

17. J. M. Ziman, " Models of Disorder," Cambridge University Press, Cambridge (1979).

18. R. E. Gibson and O. H. Leoffer, J. Am. Chem. Soc., **63**, 898 (1941).

19. T. Moriyoshi and H. Inubushi, J. Chem. Thermodyn., **9**, 587 (1977).

20. O. Kiyohara and G. C. Benson, J. Solution Chem., **10**, 281 (1981).

21. M. Diaz Peña and G. Tardajos, J. Chem. Thermodyn., **11**, 441 (1979).

22. B. P. Sahil, H. Gager and A. J. Richard, J. Chem. Thermodyn., **8**, 179 (1976).

23. M. Sakurai, J. Solution Chem., **17**, 267 (1988).

24. G. C. Benson and O. Kiyohara, J. Solution Chem., **9**, 791 (1980).

25. K. Nishikawa and T. Iijima, Bull. Chem. Soc. Jpn., **57**, 1750 (1984).

26. G. Walter and P. W. Schmidt, J. Appl. Cryst., **14**, 28 (1981).

27. G. Porod, "Small Angle X-ray Scattering," ed O. Glatter and O. Kratky, Academic Press, London (1982), ch. 2.

Chapter 3

A New Parameter Reflecting the Shape of SAXS Curve: χ

3.1 Introduction

At small scattering angles, the SAXS intensity curve obtained from an isotropic sample (I(s)) can be approximated by the following polynomial:[1]

$$I(s) = r_0 - r_2 s^2 + r_4 s^4 - r_6 s^6 + \cdots, \qquad (3\text{-}1)$$

where

$$r_{2i} = (1/(2i+1)!) \int \langle \Delta\rho_e(0)\Delta\rho_e(r)\rangle\, r^{2i}\, 4\pi r^2\, dr. \qquad (3\text{-}2)$$

Here, s is the scattering parameter ($s = 4\pi \sin\theta/\lambda$, 2θ: scattering angle, λ: wavelength of X-rays), $\Delta\rho_e(r)$ is the difference in the electron density from the average at the position r, and $\langle \cdots \rangle$ denotes the ensemble average. The 'moment' determined through a SAXS measurement (r_{2i}) reflects various aspects of microinhomogeneity in the solution. The zero-angle X-ray scattering (I(0)) is equal to r_0. The concentration fluctuation[2] and the Kirkwood-Buff parameters[3] can be obtained from r_0 (=I(0)). The Debye's correlation length (L_D)[4] is defined by $(3! \cdot r_2/r_0)^{0.5}$.[5] The so-called correlation length (ξ) is related to r_0 and r_2 as $(r_2/r_0)^{0.5}$.[5] The chief concern in previous SAXS studies of the aqueous organic solutions is these two (r_0 and r_2).

Bale, et al.,[6] who first measured SAXS spectra of aqueous solutions as far as the author knows, investigated the concentration dependence of I(0) values of t-butyl alcohol (TBA) aqueous solutions. They compared I(0) values thus obtained

experimentally with those calculated from thermodynamic data using the Kirkwood and Buff solution theory[3] and found a good agreement between their experimental and theoretical results. Donkersloot[7] measured the concentration dependence of I(0) values of methanol aqueous solutions and the measured intensities agreed fairly well with those calculated from the theories. He also obtained experimentally the Kirkwood-Buff parameters[3] from the I(0) values of methanol/ethanol aqueous solutions.[8] Koga[9] studied SAXS spectra of TBA aqueous solutions and derived concentration fluctuations of the mixtures from the I(0) values by using the Bhatia and Thornton theory.[2] He also obtained the ξ values for several TBA aqueous solutions by applying the Ornstein and Zernike theory to his experimental data.[10] Nishikawa, et al.[11] derived concentration fluctuation, fluctuation in particle numbers,[2] and the Kirkwood-Buff parameters from the I(0) data of TBA aqueous solutions at room temperature and discussed the mixing state of the solutions using these parameters. They[5] investigated the temperature dependence of the mixing state of TBA aqueous solutions by means of SAXS on the basis of the fluctuation parameters obtained from I(0) and L_D[4] determined from the slope of the SAXS intensity curve. By using the same technique, Hayashi, et al. studied the mixing state of 1-propanol (abbreviated to NPA) aqueous solutions at room temperature.[12] They studied also the mixing state of 2-propanol aqueous solutions at room temperature on the basis of I(0) and L_D data.[12]

For understanding complicated mixing states of aqueous organic solutions, it is required to use as many kinds of indicators of microInhomogeneity as possible. Thus, the author attempts to apply the coefficients r_4, not employed in previous analyses, to studying the mixing state of the aqueous organic solutions. Here, it should be mentioned that the light scattering method has an advantage to be able to evaluate I(0) more accurately because of small s in nature, but the method is not adequate for determining the higher order coefficients, because the method can not cover a wide s range.

A constructed point-focusing SAXS diffractometer improved intensity and resolution as shown in Chapter 2. By using this diffractometer, it became possible to accurately determine higher order coefficients as well as the r_0 and r_2 in the polynomial expansion shown in eq. (3-1). Accordingly, a new parameter (χ) is proposed:

$$\chi = r_0 \cdot r_4 / r_2^2. \qquad (3\text{-}3)$$

The physical meaning of this dimensionless parameter is discussed in the next section.

3.2 Physical Meaning of χ

Being related to r_4, χ reflects the shape of I(s). To clarify the physical meaning of χ more deeply, let us compare the following theoretical SAXS functions: the exact function for spheres with a uniform size dispersed in a continuous medium ($I_S(s)$), the Guinier function ($I_G(s)$), and the Ornstein-Zernike

function ($I_{OZ}(s)$). Here, $I_G(s)$ is an approximate function for particles characterized by the radius of gyration (R_G). $I_S(s)$ and $I_G(s)$ are commonly employed for analyses of SAXS from colloidal and micellar systems and $I_{OZ}(s)$ is often used for the SAXS data analysis of critical solutions. $I_S(s)$ is given as follows:[1]

$$I_S(s) = I(0)[3\{\sin(sR_0) - (sR_0)\cos(sR_0)\}/(sR_0)^3]^2, \qquad (3\text{-}4)$$

where R_0 is the radius of the sphere. $I_G(s)$ is expressed as follows:[1]

$$I_G(s) = I(0)\exp(-R_G^2 s^2/3), \qquad (3\text{-}5)$$

and $I_{OZ}(s)$ is written as follows:[10]

$$I_{OZ}(s) = I(0)/(1+(\xi s)^2), \qquad (3\text{-}6)$$

where ξ is the so-called correlation length,[10] which is related to the Debye's correlation length L_D by $\xi = L_D/6^{0.5}$.[5]

$I_S(s)$ can be expanded for $s \cdot R_0 < 1$ as

$$I_S(s) = I(0)[1 - (R_0^2/5)s^2 + (19R_0^4/1400)s^4 - \cdots]. \qquad (3\text{-}7)$$

The χ of $I_S(s)$ is, thereby, given to be $19 \cdot 25/1400$, about 0.34. $I_G(s)$ and $I_{OZ}(s)$ are a Gaussian and a Lorentzian functions, respectively, and therefore, the χ values of $I_G(s)$ and $I_{OZ}(s)$ are 0.5 and 1.0, respectively.

The correlation functions for $I_S(s)$, $I_G(s)$, and $I_{OZ}(s)$ can be expressed analytically as follows:[1,10]

$$<\Delta\rho_e(0)\Delta\rho_e(r)>_S \propto 1 - (3/2)(r/2R_0) + (1/2)(r/2R_0)^3, \quad (3\text{-}8)$$

$$<\Delta\rho_e(0)\Delta\rho_e(r)>_G \propto \exp[-3r^2/(2R_G)^2], \quad (3\text{-}9)$$

and

$$<\Delta\rho_e(0)\Delta\rho_e(r)>_{OZ} \propto \exp(-r/\xi)/r. \quad (3\text{-}10)$$

These functions are shown in Fig. 3-1 in the form of $4\pi r^2<\Delta\rho_e(0)\Delta\rho_e(r)>$. $4\pi r^2<\Delta\rho_e(0)\Delta\rho_e(r)>_S$, $4\pi r^2<\Delta\rho_e(0)\Delta\rho_e(r)>_G$, and $4\pi r^2<\Delta\rho_e(0)\Delta\rho_e(r)>_{OZ}$ have a maximum at $(r/2R_0) = 0.525$, $r = (4/3)^{0.5}R_G$, and $r = \xi$, respectively. The values of R_G and ξ in Fig. 3-1 were determined in such a way that the positions of the maxima appeared at the same r value.

The difference among these functions lies in the decay at large r, as observed in Fig. 3-1. Here, the steep/gradual decay curve of the correlation functions should represent the clear/obscure boundary of the fluctuating structure. Since $\chi = 0.34$ for $I_S(s)$, $\chi = 0.5$ for $I_G(s)$, and $\chi = 1.0$ for $I_{OZ}(s)$, χ serves as an indicator of the sharpness of the boundary. The physical meaning of the boundary of the spheres is self-evident, and that of the structures expressed by eqs. (3-5) and (3-6) corresponds to the size-dispersion of aggregates or clusters formed in solution. Hence, χ can be regarded as an indicator for the size-dispersion of clusters, and a large/small χ value indicates a large/small size-dispersion of the clusters in solution.

In Chapters 4 and 5, I(s) curves for several aqueous organic

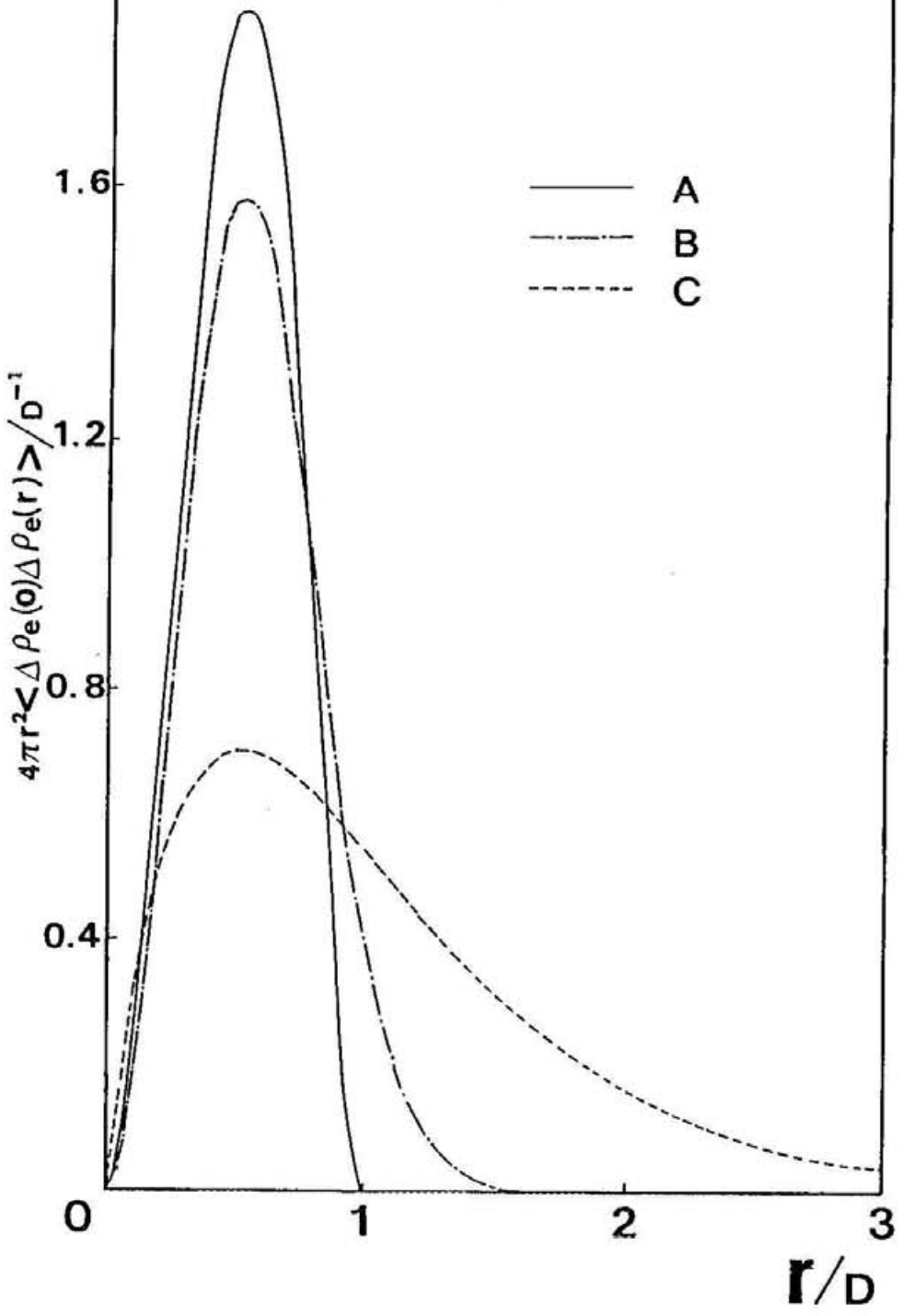

Figure 3-1. The theoretical correlation functions. A, B, and C show $4\pi r^2 \langle \Delta\rho_e(0)\Delta\rho_e(r)\rangle_S$, $4\pi r^2 \langle \Delta\rho_e(0)\Delta\rho_e(r)\rangle_G$, and $4\pi r^2 \langle \Delta\rho_e(0)\Delta\rho_e(r)\rangle_{OZ}$, respectively. Here D is the diameter of sphere: $D = 2R_0$.

solutions will be analyzed by using χ. It should be noted here that the analysis by using χ is based on a polynomial expansion shown by eq. (3-1) and the expansion is valid only for $s^2 \cdot (r_2/r_0) = s^2 \cdot \xi^2 < 1$. Since the maximum $s \cdot \xi$ is 0.8 in the present work, the use of eq. (3-1) and the analysis by using χ are thus justified.

References

1. G. Porod, "Small Angle X-ray Scattering," ed O. Glatter and O. Kratky, Academic Press, London (1982), 17.
2. A. B. Bhatia and D. E. Thornton, Phys. Rev., B **2**, 3004 (1970).
3. J. G. Kirkwood and F. P. Buff, J. Chem. Phys., **19**, 774 (1951).
4. P. Debye, J. Chem. Phys., **31**, 680 (1959).
5. K. Nishikawa, H. Hayashi, and T. Iijima, J. Phys. Chem., **93**, 6559 (1989).
6. H. D. Bale, R. E. Shepler, and D. K. Sorgen, Phys. Chem. Liquids, **1**, 181 (1968).
7. M. C. A. Donkersloot, Chem. Phys. Lett., **60**, 435 (1979).
8. M. C. A. Donkersloot, J. Solution Chem., **8**, 293 (1979).
9. Y. Koga, Chem. Phys. Lett., **111**, 176 (1984).
10. J. M. Ziman, "Models of Disorder," Cambridge University Press, Cambridge (1979).
11. K. Nishikawa, Y. Kodera, and T. Iijima, J. Phys. Chem., **91**, 3694 (1987).
12. H. Hayashi, K. Nishikawa, and T. Iijima, J. Phys. Chem., **94**, 8334 (1990).

Chapter 4

SAXS Curve Shape Analysis of 2-Butoxyethanol Aqueous Solutions by Using χ

4.1 Introduction

A dimensionless parameter (χ) has been proposed and its physical meaning has been discussed in Chapter 3. χ reflects the shape of SAXS curve.

In this chapter, the SAXS curve shape of 2-butoxyethanol (BE) aqueous solutions under various conditions is analyzed by the use of χ as well as the so-called correlation length (ξ).[1] BE aqueous solution has a lower critical solution temperature (LCST) near room temperature[2,3] and its correlation length and fluctuation parameters show very large variations with temperature and concentration.[2,4] Hence, the solution is a suitable system to examine whether or not an analysis of the SAXS curve shape in terms of χ is adequate to understand the mixing state of aqueous organic solutions.

4.2 Experimental

BE aqueous solutions were prepared by weighing the components. Water was deionized and distilled. BE of reagent grade with a 99.9% purity was used after drying with molecular sieves (3A 1/8, Aldrich). Each sample was kept in a cell with about 0.1 mm-thick mica windows. The thickness of the sample was 2.5 mm.

Measurements of SAXS on each sample were performed by the diffractometer shown in Chapter 2. The temperature of each sample was kept constant within 0.5 °C by using a cell holder coupled to a bath circulator. The accumulation times of a measurement for samples were 10000 - 20000 s.

The data were corrected for background scattering, multiple scattering, Compton scattering, and absorption according to the manner described in Chapter 2. They were subsequently converted into an absolute scale.

The SAXS curve (I(s)) can generally be approximated by the following Ornstein-Zernike equation ($I_{OZ}(s)$) for $\xi \cdot s << 1$:[5]

$$I_{OZ}(s) = I(0)/(1+(\xi s)^2). \qquad (3\text{-}6)$$

Thus, ξ can be determined from an Ornstein-Zernike plot of $I^{-1}(s)$ vs. s^2:[6]

$$I^{-1}(s) = 1/I(0) + (\xi^2/I(0))s^2. \qquad (4\text{-}1)$$

Then, each I(s) in the region $\xi \cdot s < 0.8$ was approximated to be expressed as the polynomial function shown by eq. (3-1), and the coefficients (r_{2i}) were determined by using a least-squares calculation. The R-factor defined in eq. (2-4) did not exceed 0.0001 in all data. From these r_{2i} values, χ was calculated according to eq. (3-3).

4.3 Results & Discussion

Figure 4-1 shows a part of the miscibility curve of BE aqueous solutions[2] as well as the measured points in the present SAXS study. The LCST is ca. 49 °C.[2,3] Somewhat different values have been reported as the critical composition; 5.98[3] and 7 mol%.[2]

The ξ values determined in the present study are plotted against the BE mole fraction C_1 in Fig. 4-2. ξ is largest

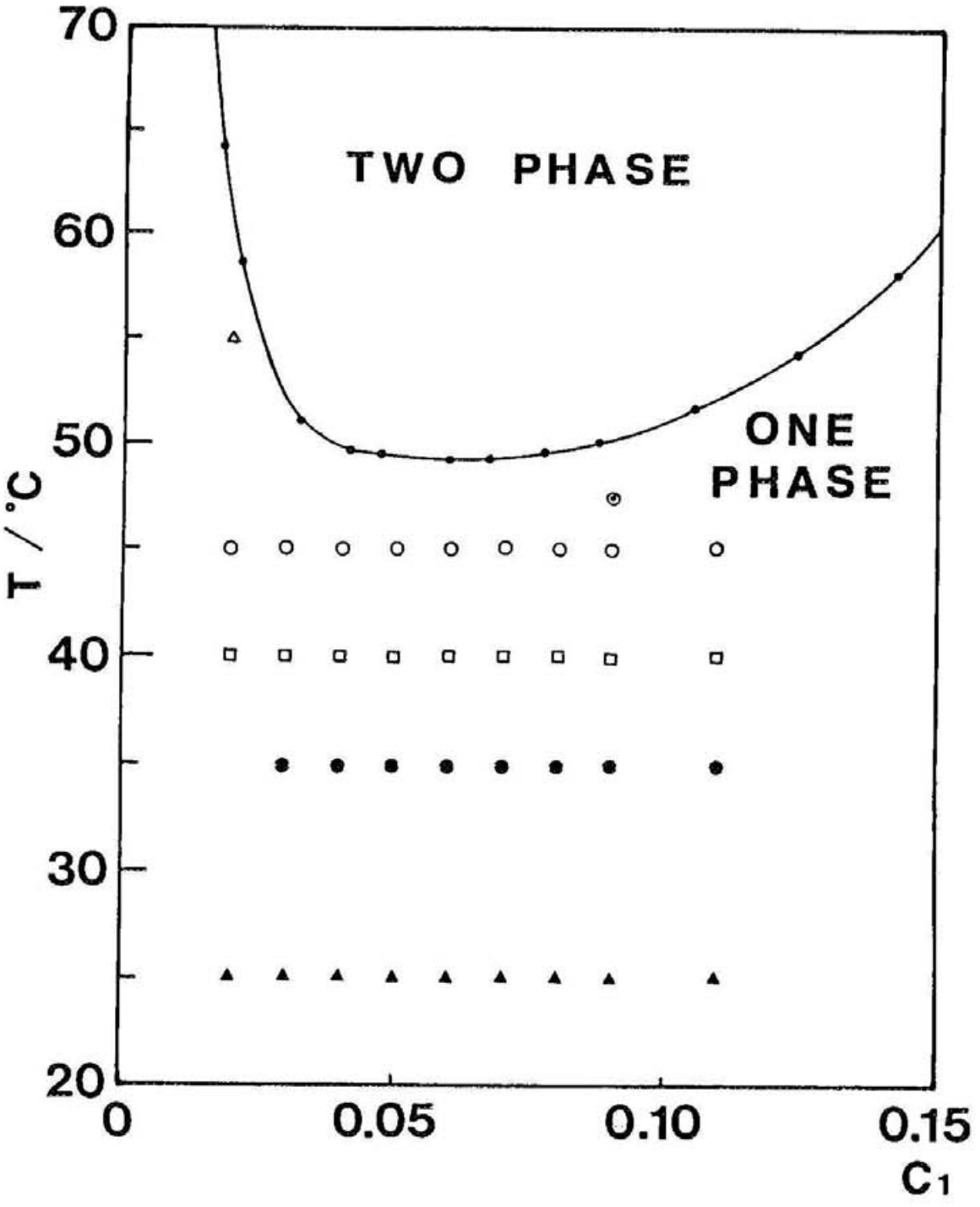

Figure 4-1. Miscibility curve of BE aqueous solutions from ref. 2 and the measured points in the present work.

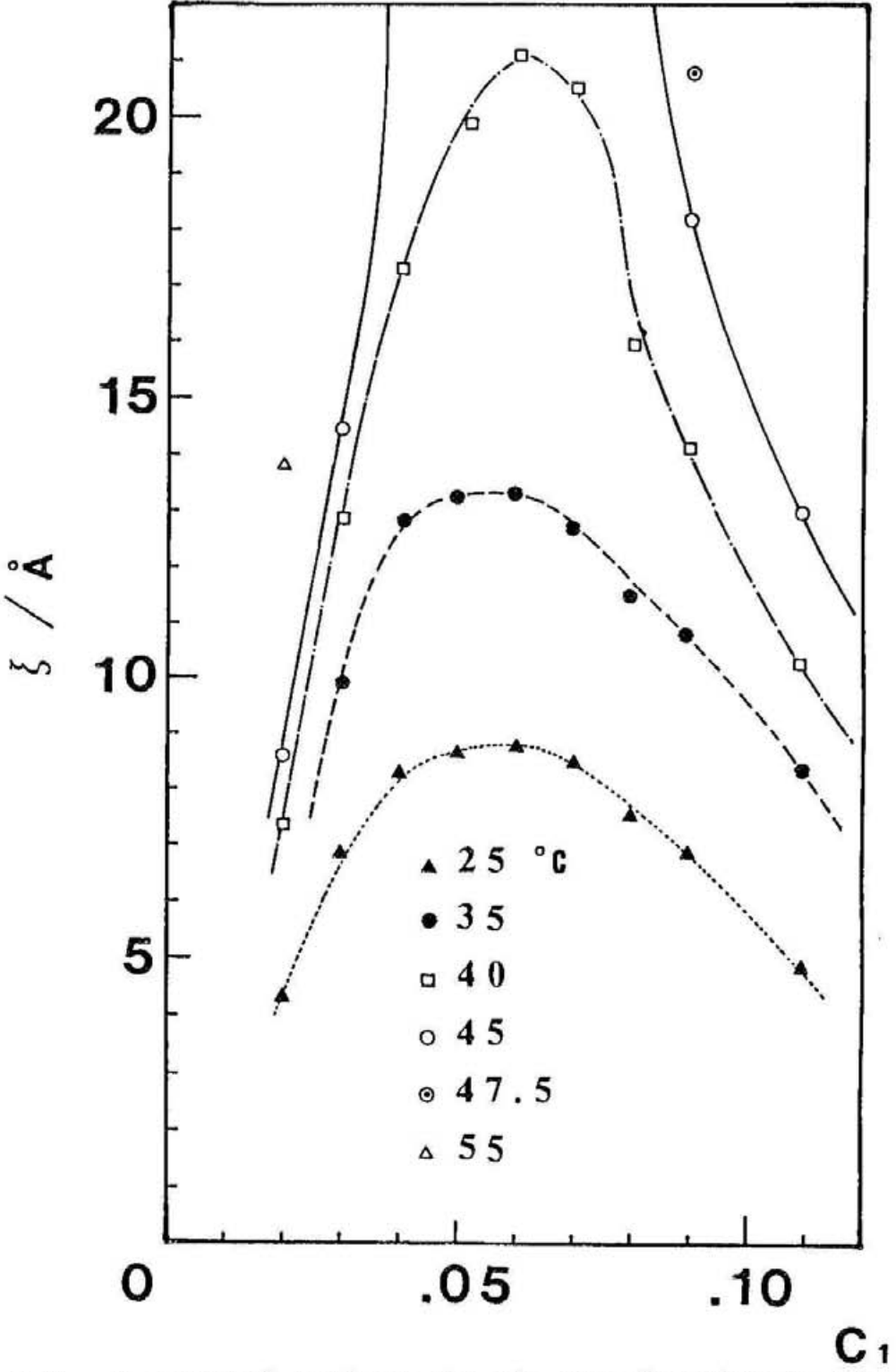

Figure 4-2. ξ plotted against the BE mole fraction C_1 at various temperatures.

near the critical composition (BE 5 - 7 mol%) and shows a marked increase with temperature rise at all the concentrations studied. In particular, under the conditions very close to the LCST, ξ becomes too large to be evaluated accurately the value by the present SAXS diffractometer (the minimum s value measured is 0.03 $\mathring{A}^{-1}$).

χ values are plotted against C_1 in Fig. 4-3. Contrary to ξ, χ is smallest (about 0.8) near the critical composition at all the temperatures studied. At off-critical compositions, χ is much larger, but sharply decreases with temperature rise and becomes almost 0.8 near the miscibility curve in Fig. 4-1.

Several studies have been performed concerning the mixing state of BE aqueous solutions. It has been concluded from Rayleigh and Raman scattering that two types of clusters are formed in BE aqueous solutions depending on the concentration; clathrate hydrate-like $g[(H_2O)_{50}BE]$ and aggregate $h[(H_2O)_4BE]$.[2] The numbers g and h increase with temperature rise, eventually leading to phase separation. In accordance with this, an increase in ξ at high temperatures has been observed from a dynamic light scattering study at 23 and 42 °C.[4] The temperature dependence of ξ shown in Fig. 4-2 more decisively illustrates cluster growth with temperature rise, although the form of the clusters can not be specified.

In addition to ξ, an analysis of SAXS curves in terms of χ provides another piece of information about the clusters formed. In Chapter 3, this parameter has been interpreted to represent

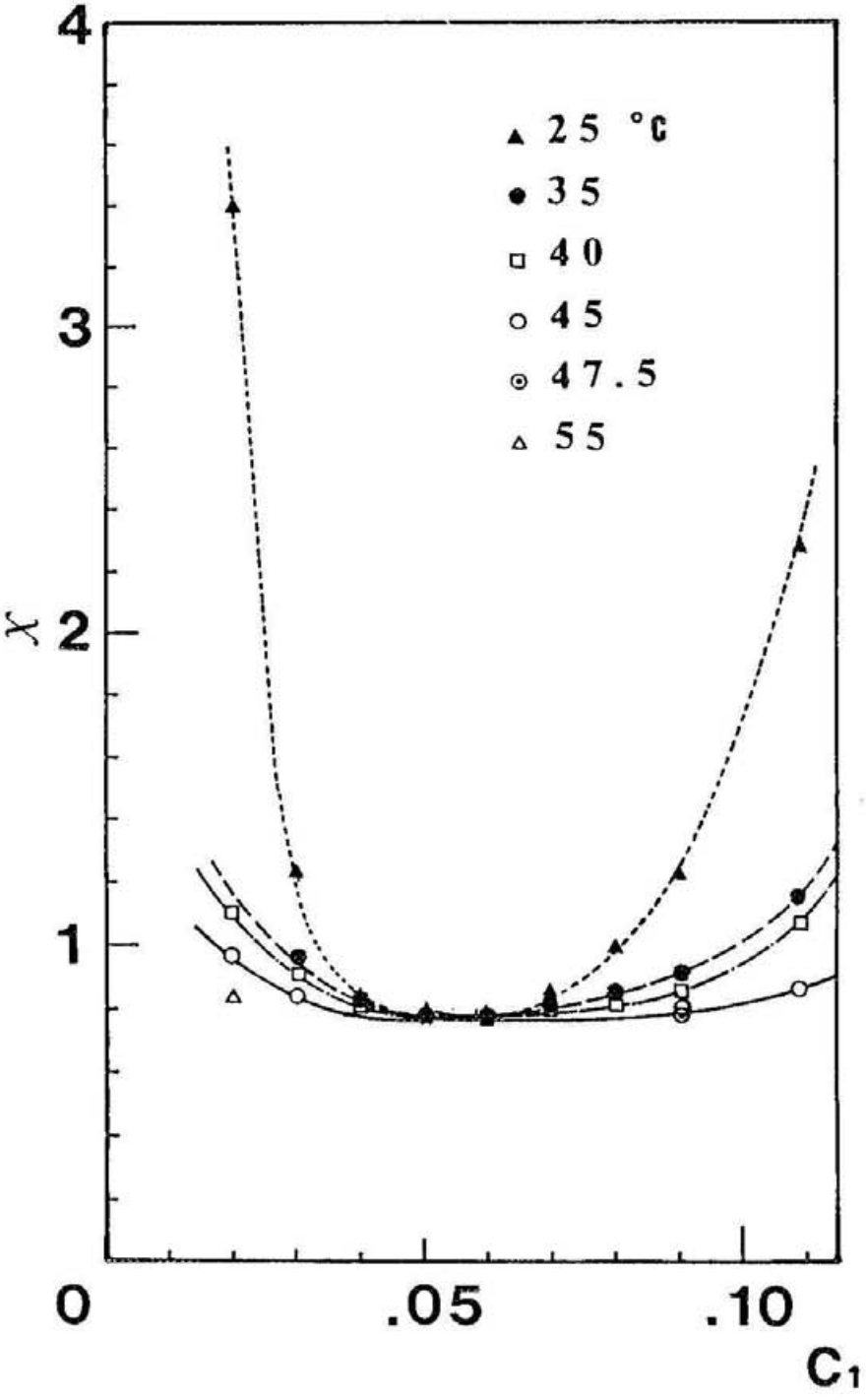

Figure 4-3. χ plotted against the BE mole fraction C_1 at various temperatures.

the size dispersion of fluctuating clusters formed in solution; a large/small χ correspond to a large/small size dispersion. Hence, the results illustrated in Fig. 4-3 show that, near the critical composition (around 5 mol%), clusters having a fairly well-defined size are formed at all the temperatures studied, because χ is always small and is about 0.8. The size depends on temperature and increases with temperature rise as is indicated by ξ.

On the other hand, at higher or lower concentrations than the critical composition, χ becomes very large at room temperature and ξ is only about 5 $\mathring{A}$, meaning that clusters, if exist at all, are not well-defined. With temperature rise, however, χ becomes smaller, accompanied by an increase of ξ. That is, well-defined size clusters become dominant and they grow with temperature rise.

It is known that the I(s) near the critical condition is expressed by the Ornstein-Zernike (OZ) function (eq. (3-6)) over a relatively wide region of $\xi \cdot s$ ($\xi \cdot s < 3^5$ or 4^3). In that case, χ is calculated to be 0.8.[7] χ is experimentally observed to be 0.8 not only near the critical condition (LCST) but also near the miscibility curve and below the LCST. These facts suggest that I(s) of off-critical solutions may also be approximated by the OZ equation, if some conditions are satisfied. Indeed, the OZ equation has been found to be adequate to express I(s) of t-butyl alcohol (TBA) aqueous solutions for a concentration range (from TBA 6.96 mol% to 29.68 mol%)[8] and employed to analyze I(s) of

SANS (small-angle neutron scattering) near the miscibility curve of K/KBr molten solutions.[6]

4.4 Conclusions

The SAXS data of 2-butoxyethanol aqueous solutions have been measured over wide concentration and temperature ranges and analyzed with a polynomial expansion by taking up to the 4-th order term into consideration.

It has been experimentally shown that χ, which reflects the SAXS curve shape, is very sensitive to the mixing state and accordingly may be employed as a useful parameter.

References

1. J. M. Ziman, "Models of Disorder," Cambridge University Press, Cambridge (1979).
2. N. Ito, T. Fujiyama, and Y. Udagawa, Bull. Chem. Soc. Jpn., **56**, 379 (1983).
3. C. Baaken, L. Belkoura, S. Fusenig, Th. Müller-Kirschbaum, and D. Woermann, Ber. Bunsenges. Phys. Chem., **94**, 150 (1990).
4. T. Kato, J. Phys. Chem., **89**, 5750 (1985).
5. Y. Izumi, Phys. Rev., A **39**, 5826 (1989).
6. J. F. Jal, P. Chieux, and J. Dupuy, J. Appl. Cryst., **11**, 610 (1978).
7. In the case of a Lorentzian χ must be equal to 1. Owing to the truncation effect, however, χ is calculated to be 0.8 if expanded between $0.03 < s < (0.8/\xi)$.
8. Y. Koga, Chem. Phys. Lett., **111**, 176 (1984).

Chapter 5

Mixing States of 1-Propanol Aqueous Solutions Studied by SAXS

5.1 Introduction

1-Propanol (abbreviated to NPA hereafter) aqueous solution is one of the most notable systems in the study of mixing states. The aqueous solution has no critical temperature in spite of its relatively large microinhomogeneity. Recently, several measurements of the microinhomogeneity in this solution have been performed using ultrasonic absorption,[1] light scattering,[2] small-angle neutron scattering (SANS),[3] and small-angle X-ray scattering (SAXS) methods.[4] Details of the microinhomogeneity are, however, not clear yet. This is in part due to either the insufficient range of the concentration and temperature employed in previous studies, or to a lack of measures of microinhomogeneity. In this chapter, the mixing state of NPA aqueous solutions is discussed in terms of the concentration fluctuation and correlation length, as well as χ, derived from SAXS data obtained over wide concentration and temperature ranges.

5.2 Experimental

NPA aqueous solutions of ten different concentrations (mole fractions of NPA: C_1) were prepared by weighing the components: C_1 = 0.051, 0.071, 0.089, 0.111, 0.122, 0.137, 0.167, 0.200, 0.253, and 0.299. Water was deionized and distilled. NPA of reagent grade with a 99.9% purity was used after drying with molecular sieves (3A 1/8, Aldrich). Each sample was kept in a cell with about 0.1 mm-thick mica windows.

Measurements of the SAXS spectra on each sample were

performed at 15, 25, 35, and 40° C. The temperature of each sample was kept constant within 0.5° C by using a cell holder coupled to a bath circulator. The diffractometer shown in Chapter 2 was used for the SAXS measurements. The accumulation times of one measurement were 10000 - 20000 s.

The data were corrected for background scattering, multiple scattering, Compton scattering, and absorption. They were subsequently converted into an absolute scale by using the value obtained in Chapter 2. Zero-angle X-ray scattering (I(0)) and correlation length (ξ) were determined from an Ornstein-Zernike plot.[5] Then, each SAXS intensity curve (I(s)) in the region $\xi \cdot s < 0.8$ was approximated by using eq. (3-1), and the coefficients (r_{2i}) were determined by a least-squares calculation. From these r_{2i}, χ was calculated according to eq. (3-3).

5.3 Results

The temperature dependence of I(0) is shown in Fig. 5-1. The magnitude of the error in the I(0) value was estimated to be 3%. By using I(0), together with the isothermal compressibility and partial molar volumes, the mean square fluctuation in concentration ($\langle N \rangle \langle (\Delta C_1)^2 \rangle$) shown in Fig. 5-2 and other fluctuation parameters could be obtained, as was described in ref. 6. Here, N is the total particle number. The phrase "mean square" is omitted hereafter. The partial molar volumes and isothermal compressibilities at 15, 25, and 35° C were calculated from the data of Benson and Kiyohara.[7-9] The fluctuation parameters at 40 ° C were not obtained because of a lack of data

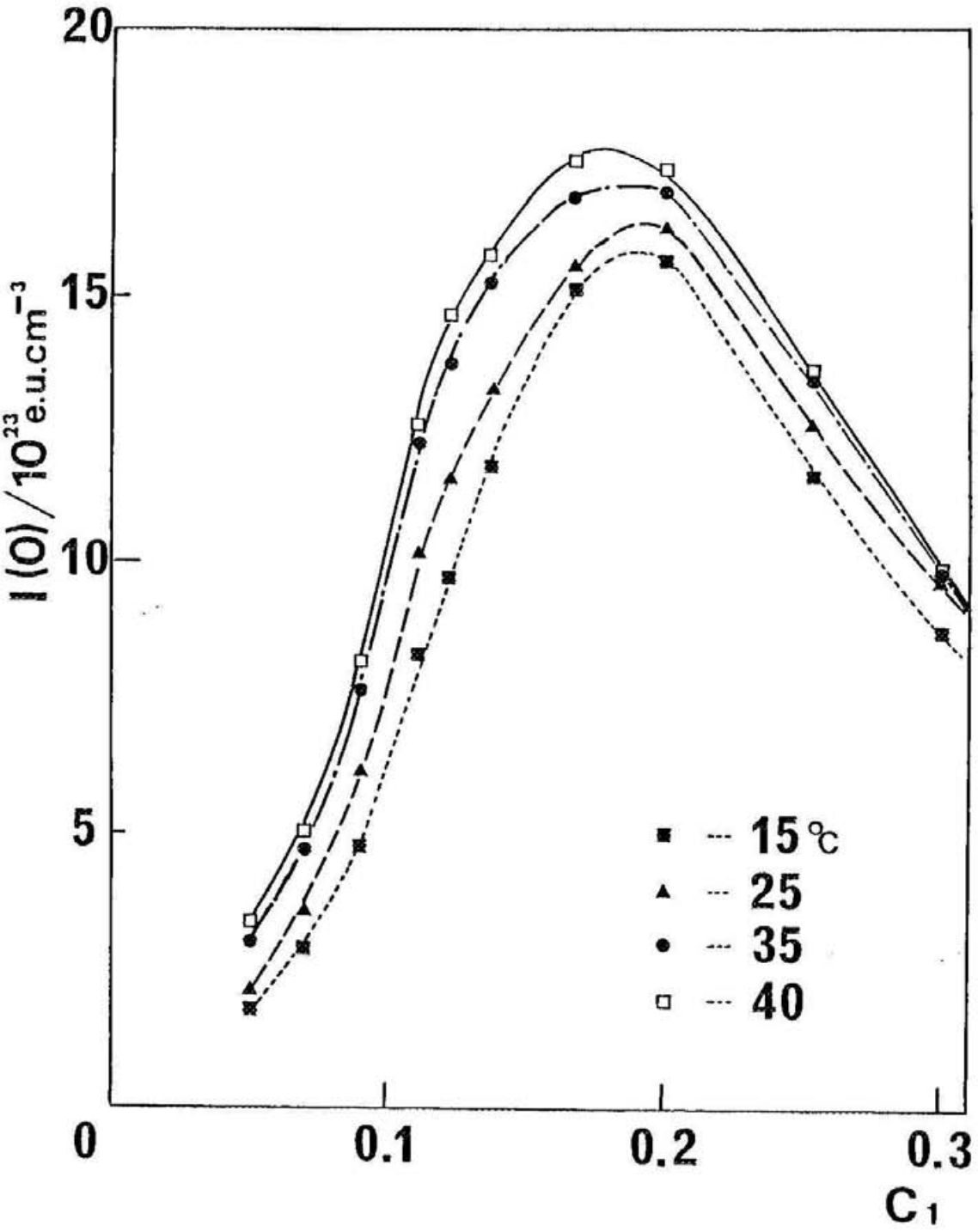

Figure 5-1. Temperature dependence of the zero-angle X-ray scattering intensity plotted against the mole fraction of NPA (C_1).

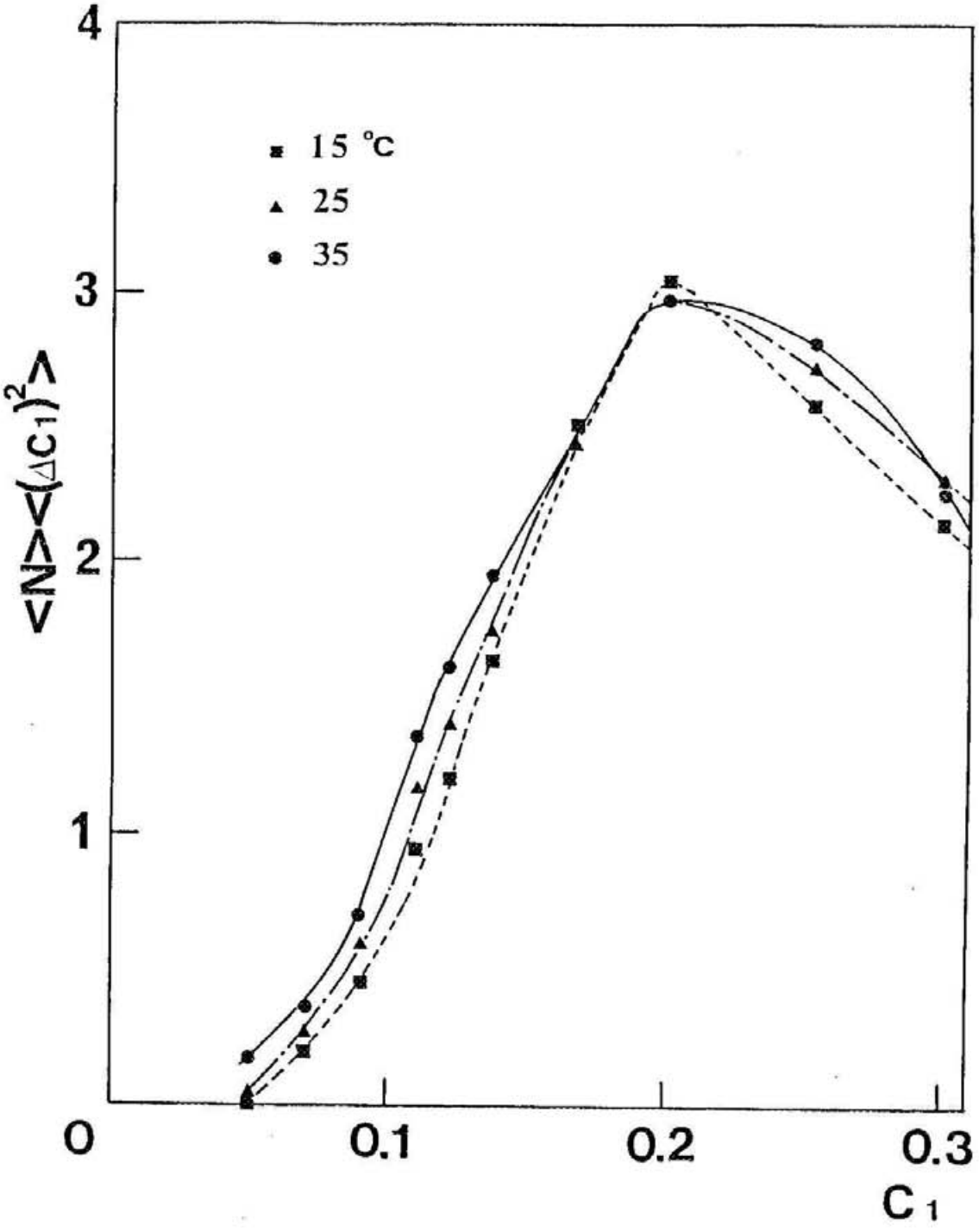

Figure 5-2. Temperature dependence of concentration fluctuation of NPA aqueous solutions.

concerning the partial molar volumes. The total magnitude of the error in $\langle N \rangle \langle (\Delta C_1)^2 \rangle$ was estimated to be 5%.

The temperature dependences of ξ and χ are shown in Figs. 5-3 and 5-4, respectively. The ξ value calculated from the SANS data[3] (at C_1= 0.114, at 25° C), which is in good agreement with ours, is also shown in Fig. 5-3.

$\langle N \rangle \langle (\Delta C_1)^2 \rangle$ shows no marked temperature dependence and varies with concentration with a maximum at about 20 mol%. ξ is essentially independent of temperature and varies only slightly with concentration, having a small maximum at about 15 mol%. On the other hand, χ depends on both temperature and concentration and shows different temperature dependences at higher and lower concentrations than about 15 mol%. Hence, NPA aqueous solutions can be classified by using χ into the following three concentration regions:

(a) C_{low}: ($C_1 < 0.12$). In this concentration region, the χ values are relatively large and decrease with either an increase in the temperature or concentration.

(b) C_{middle}: ($0.12 < C_1 < 0.20$). In this concentration region, the χ values are relatively small, and insensitive to the temperature and concentration. $\langle N \rangle \langle (\Delta C_1)^2 \rangle$ and ξ take maximum values at each temperature in this region.

(c) C_{high}: ($C_1 > 0.20$). In this concentration region, the χ values are relatively large and increase with either increase in the temperature or concentration.

5.4 Discussion

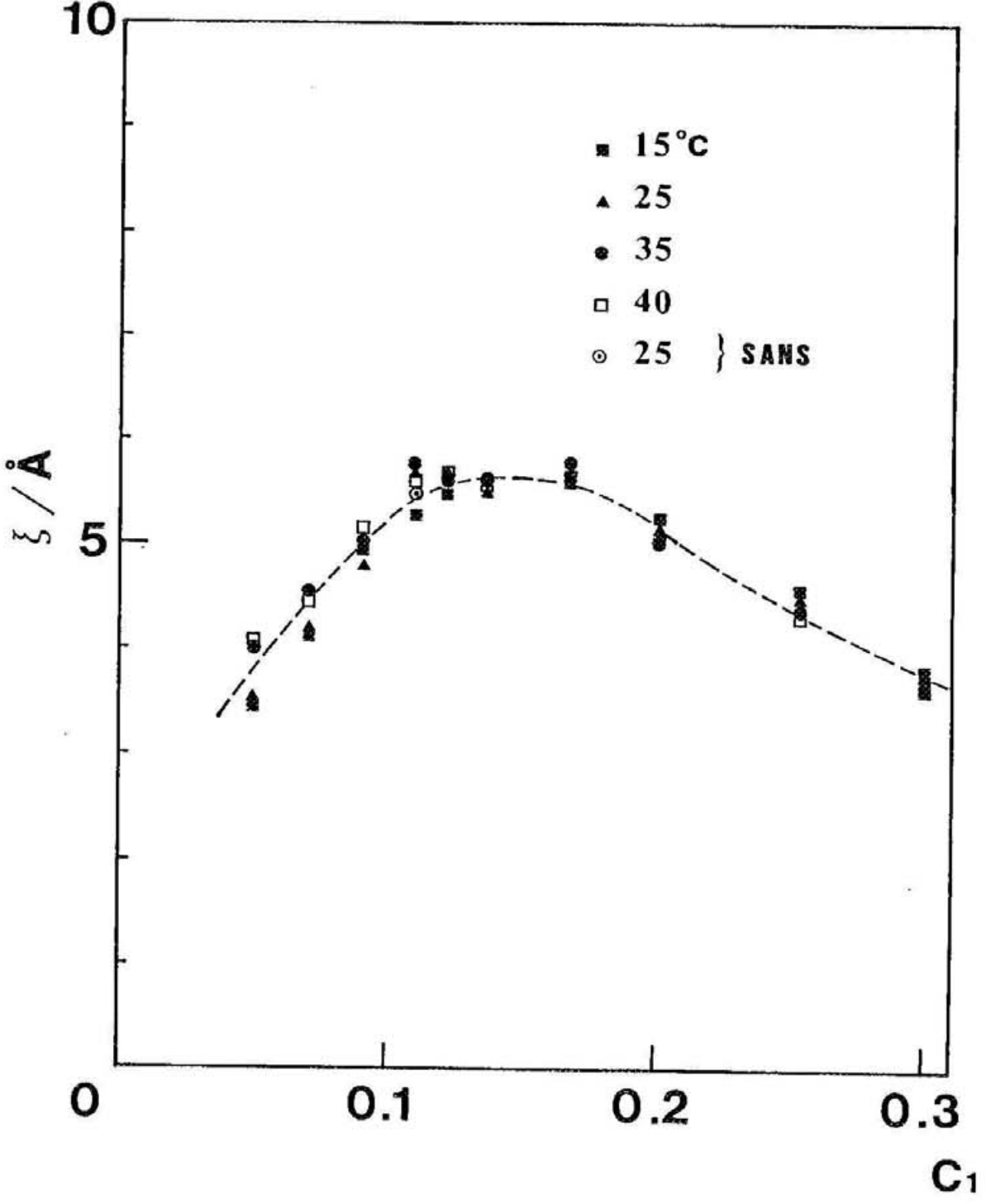

Figure 5-3. Temperature dependence of the correlation length ξ with the mole fraction of NPA (C_1).

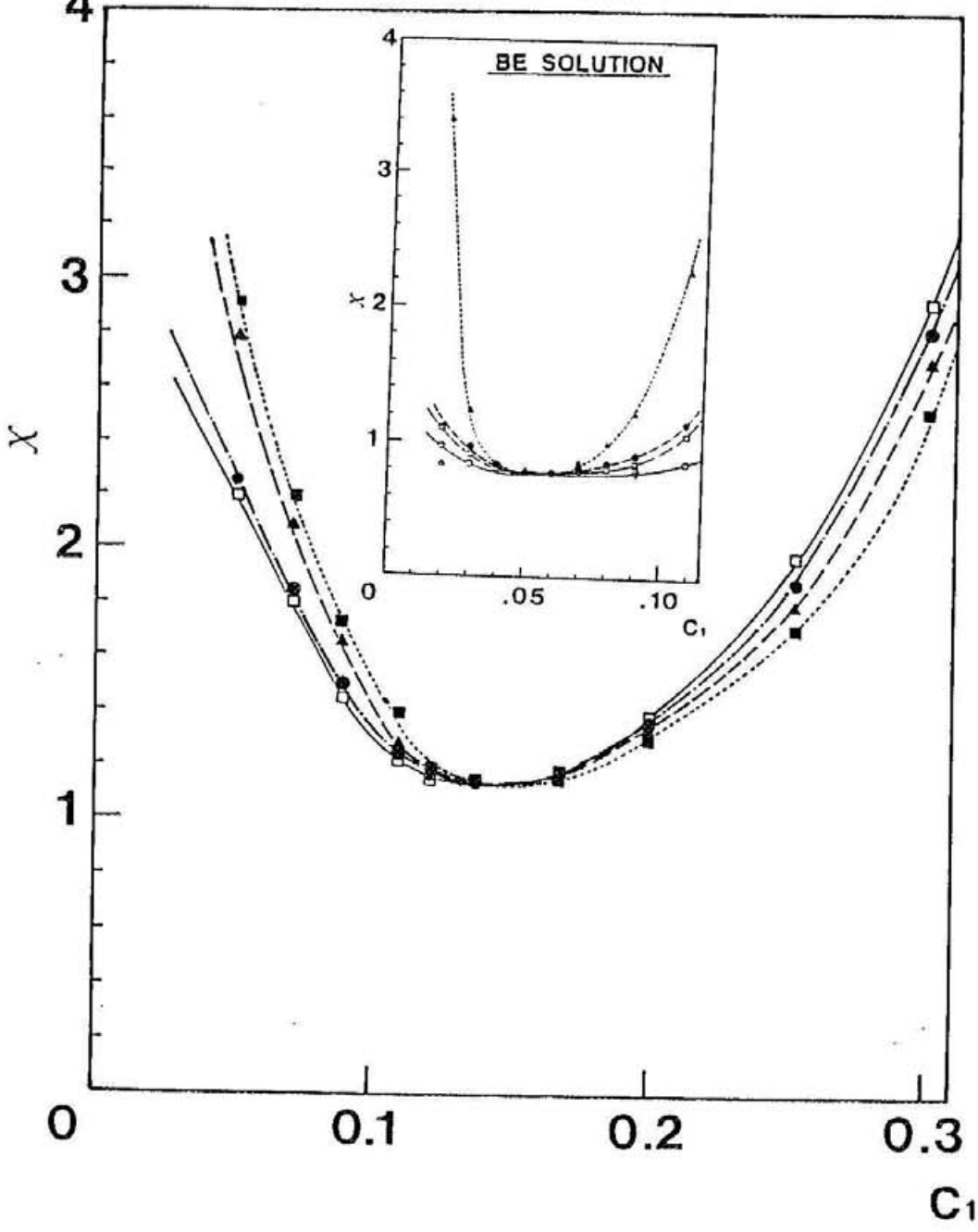

Figure 5-4. χ plotted against the mole fraction of NPA (C_1) at various temperatures. Inserted is plots in the BE aqueous solution system for comparison as have been shown in Fig. 4-3. ■: 15, ▲: 25, ●: 35, □: 40, ○: 45, ⊙: 47.5, and △: 55° C.

The mixing states of NPA aqueous solutions can be classified by χ into three regions: C_{low}, C_{middle}, and C_{high}.

In the C_{middle} region, $\langle N \rangle \langle (\Delta C_1)^2 \rangle$ and ξ show maxima and χ takes a minimum. The results suggest that the microinhomogeneity is large and has a sharp boundary. Hence, the formation of some kind of aggregates is expected.

A large microinhomogeneity characterized by a large concentration fluctuation and a long correlation length has been observed in several aqueous solutions of nonionic amphiphiles with relatively short hydrophobic tails, e.g., NPA,[1-4] t-butyl alcohol (TBA),[10-12] 2-butoxyethanol (BE),[3,13,14] and tetrahydrofuran (THF).[15] The mixing states of these solutions have been described by assuming either clathrate hydrate-like aggregates (TBA, BE, and THF) or micelle-like aggregates (NPA and BE); such aggregate formation must also be the origin of the observed microinhomogeneity.

Although it is not possible to determine which is the case for the NPA solutions, a micelle-like aggregate is more likely than a clathrate hydrate because of the molecular structure; the hydrophobic tail of NPA without a branch should work effectively for a hydrophobic interaction, while a large distortion of the hydrogen bond is required if an NPA molecule is caged by water molecules.[4]

Grossmann and Ebert (GE) found that various physical properties, such as the translational diffusion constant and the hydrodynamic radius of a cluster, show either a maximum or a

minimum at a molar ratio of 1 NPA and 5 water (ca. NPA 17 mol%), and they proposed the existence of micelle-like aggregates comprising $(n\text{-}C_3H_7OH)_8(H_2O)_{40}$ with a diameter of 16 Å.[2] Although this model is considered to be qualitatively correct, a more detail picture of the aggregates should be given in view of the present SAXS study with various reasons in the following. First, although the formation of aggregates with a uniform size proposed by GE must lead to an extremely small concentration fluctuation,[4] the fluctuation experimentally found is fairly large and close to the maximum at the concentration of ca. NPA 17 mol%, as shown in Fig. 5-2. Second, the χ value is about 1.1, suggesting that the sizes of aggregates are not uniform. For a system comprising spheres of a uniform size dispersed in a continuous medium, χ was calculated to be 0.34 (as described in Chapter 3). For the analysis of I(s) from micellar systems, $I_G(s)$ has been usually used.[16] In this case χ is 0.5, which is still much smaller than the observed value, 1.1. Thus, the size dispersion among micelle-like aggregates is concluded in the NPA solution in the C_{middle} region; it should be much larger than that of ordinary micelles.

The temperature dependence of an aggregate near NPA 17 mol% is somewhat peculiar. Micelles of nonionic amphiphiles are known to grow in size with a temperature rise,[17] and aggregates of nonionic amphiphiles such as BE, TBA, and THF have been reported to behave in a similar fashion.[3,10-15] However, no marked temperature dependence of $\langle N \rangle \langle (\Delta C_1)^2 \rangle$ and of ξ has been observed

near NPA 17 mol%, as shown in Figs. 5-2 and 5-3. In accordance with the present observation, GE also observed that the hydrodynamic radius is essentially independent of the temperature.[2] The reason for the lack of a marked temperature dependence is not clear.

In the C_{low} region, $\langle N \rangle \langle (\Delta C_1)^2 \rangle$ and ξ increase with an increase in the concentration. The trends are very similar to those observed with other aqueous solutions of amphiphiles, and the result indicates the growth of (probably micelle-like) aggregates.[4,10-12,18] The χ values at C_{low} decrease with an increase in the concentration, also suggesting the formation of aggregates with certain sizes.

In the C_{high} region, $\langle N \rangle \langle (\Delta C_1)^2 \rangle$ and ξ decrease with an increase in the concentration. χ also increases. The result means that the size of the aggregates at C_{high} decreases and the size distribution becomes wide with the concentration. The change in the size of aggregates must be due to an insufficiency in the number of water molecules available to form stable micelle-like aggregates consisting of, on the average, a molar ratio of 1 NPA to 5 H_2O.

On the other hand, there are surplus water molecules in the C_{low} region. $\langle N \rangle \langle (\Delta C_1)^2 \rangle$ is much smaller in C_{low} than in C_{high}, as shown in Fig. 5-2. This result indicates that the aggregates in C_{high} should not be the same as those in C_{low}, and that the number of water molecules forming aggregates should be larger in C_{high} than in C_{low}. The temperature dependence of χ in C_{high}

is opposite to that in C_{low} as shown in Fig. 5-4, which also indicates the difference of the aggregates.

For comparison, a χ vs. C_1 plot for BE aqueous solution (Fig. 4-3) is inserted in Fig. 5-3, where χ markedly changes with both concentration and temperature. BE aqueous solution has a lower critical solution temperature, and the ξ value becomes large with temperature rise (see Fig. 4-2). Clearly, modest/drastic local structure changes with temperature and concentration of NPA/BE are reflected by χ.

5.5 Conclusions

SAXS spectra of NPA aqueous solutions were measured over a wide concentration range at various temperatures. A parameter χ has been found to be a good indicator to study microinhomogeneity in NPA aqueous solutions, as well as in BE aqueous solutions (see Chapter 4). By using χ, the mixing states of NPA aqueous solutions can be classified into three regions, and the large microinhomogeneity around NPA 15 mol% is attributed to the formation of micelle-like aggregates.

References

1. W. M. Madigosky and R. W. Warfield, J. Chem. Phys., **86**, 1491 (1987).
2. G. H. Grossmann and K. H. Ebert, Ber. Bunsenges. Phys. Chem., **85**, 1026 (1981).
3. G. D'Arrigo and J. Teixeira, J. Chem. Soc. Faraday Trans., **86**, 1503 (1990).
4. H. Hayashi, K. Nishikawa, and T. Iijima, J. Phys. Chem., **94**, 8334 (1990).
5. J. F. Jal, P. Chieux, and J. Dupuy, J. Appl. Cryst., **11**, 610 (1978).
6. H. Hayashi, K. Nishikawa, and T. Iijima, J. Appl. Cryst., **23**, 134 (1990).
7. G. C. Benson and O. Kiyohara, J. Solution Chem., **9**, 791 (1980).
8. G. C. Benson, P. J. D'Arcy, and O. Kiyohara, J. Solution Chem., **9**, 931 (1980).
9. O. Kiyohara and G. C. Benson, J. Solution Chem., **10**, 281 (1981).
10. Y. Koga, Chem. Phys. Lett., **111**, 176 (1984).
11. K. Iwasaki and T. Fujiyama, J. Phys. Chem., **81**, 1908 (1977); **83**, 463 (1979).
12. G. W. Euliss and C. M. Sorensen, J. Chem. Phys., **80**, 4767 (1984).
13. G. Roux, G. Perron, and J. E. Desnoyers, J. Phys. Chem., **82**, 966 (1978).

14. Y. Koga, W. W. Y. Siu, and T. Y. H. Wong, J. Phys. Chem., **94**, 3879 (1990).

15. C. M. Sorensen, J. Phys. Chem., **92**, 2367 (1988).

16. G. Porod, "Small Angle X-ray Scattering," ed O. Glatter and O. Kratky, Academic Press, London, p.17 (1982).

17. C. Tanford, "The Hydrophobic Effect," Wiley, New York (1980).

18. K. Nishikawa, H. Hayashi, and T. Iijima, J. Phys. Chem., **93**, 6559 (1989).

Chapter 6

Growth of Metal Silicate Clusters in Solution Studied by SAXS

6.1 Introduction

It is well-known that the activity and selectivity of a metal-supported catalyst depend on the size of metal particle,[1] and hence, many attempts have been made to develop techniques to control the metal particle size. It was found by Ueno, et al. that catalysts with a homogeneous metal size can be obtained by hydrolysis of the mixed solutions of metal ethylene glycolates and tetraethoxysilane, $Si(OEt)_4$ (TEOS).[2] This is called the alkoxide method. In this procedure, metal is integrated into the silicate network through the formation of the metal silicate, eventually transforming to gel.[3]

$$Me\begin{matrix}/\ O\text{-}CH_2 \\ \\ \backslash\ O\text{-}CH_2\end{matrix} + Si(OEt)_4 \rightleftharpoons Me\begin{matrix}/\ O\text{-}Si(OEt)_3 \\ \\ \backslash\ O\text{-}Si(OEt)_3\end{matrix} + (CH_2\text{-}O\text{-}C_2H_5)_2 \qquad (6\text{-}1)$$

Here, Me means metal.

Structural changes at several stages of the catalyst preparation procedure have been studied by the EXAFS spectroscopy and electron microscopy.[3] Unfortunately, the three-dimensional growth of silicate polymers in the mixed solution can not be probed by these methods.

The SAXS measurement is one of the most direct ways to study the structure of polymers in solution. In a recent study, the SAXS technique has been shown to be useful to know the fractal structure and the size of polymers.[4] In this chapter, the author reports SAXS measurements of mixed solutions including nickel and iron silicates, which are typical metal silicates, and discusses

the growth of metal silicates in the solutions.

6.2 Experimental

Two kinds of solutions including nickel silicates, named NiA and NiB, were prepared as follows: 2.478 g of $Ni(NO_3)_2 \cdot 6H_2O$ was dissolved into 20 ml of ethylene glycol at 25 °C (p-1), and subsequently 28.7 ml of water was added within 2 min. after p-1 (p-2). Finally, 16.7 ml of TEOS was added within 2 min. after the p-2 at 25 °C with vigorous stirring (p-3). In the case of NiB, 0.5 ml of HNO_3 was added after p-2. A solution including iron silicates, named FeA, was also prepared in the same manner as NiA, except that 3.617 g of $Fe(NO_3)_3 \cdot 9H_2O$ was dissolved into ethylene glycol. The weight ratio, Me : SiO_2, is 1 : 9 in all samples. Water used for the preparation was deionized and distilled. Ethylene glycol and TEOS of reagent grade with a 99.9 % purity were used without further purification.

The dissolution times of TEOS were as follows: NiA = 16.7 $\pm$ 0.1 h, NiB = 0.8 $\pm$ 0.1 h, and FeA = 0.6 $\pm$ 0.1 h. Hence, SAXS of each sample before the time indicated above could not be observed. The pH values of each sample, measured by a glass electrode immediately after TEOS was dissolved, were as follows: NiA = 3.8, NiB = 0.9, and FeA = 1.0. After dissolution of TEOS, each sample was kept in a cell made of Cu having about 0.1 mm-thick mica windows. The temperature of the sample was kept at 25 $\pm$ 0.5 °C by the cell holder coupled to a bath circulator.

The gelation time t_g was determined from the time when the solution was solidified after TEOS was added into the solution:

NiA = 29 h, NiB = 185 h, and FeA = 37 h. As far as the same cell was used, the error in t_g was within 3%, but the t_g depended on the volume of the cell and showed large values for the sample in a large vessel. Hence, the present t_g values are not absolute but relative.

The diffractometer shown in Chapter 2 was used for the SAXS measurements. The s-region ranging from 0.038 to 0.40 $\mathring{A}^{-1}$ was covered by the diffractometer. The maximum length scale of the present SAXS measurement (d_{max}) was roughly estimated as $d_{max} = \lambda/(2\sin\theta_{min}) = 2\pi/s_{min} \simeq 165$ $\mathring{A}$ (s_{min} is the minimum s value, 0.038 $\mathring{A}^{-1}$). The accumulation time in a measurement was 6000 - 12000 s. The data were corrected for background scattering and absorption.

6.3 Results & Discussion

In the region $sR_G \simeq 1$, the SAXS intensity (I(s)) follows the well-known Guinier law:[5]

$$I(s) \propto \exp[(-1/3)R_G^2 s^2], \qquad (6\text{-}2)$$

where R_G is the radius of gyration of the scatterer (Guinier radius), reflecting the size of the small isolated clusters. In the later stage of the gelation, however, R_G increases and becomes sometimes comparable with the present maximum length scale. In this case what R_G means is not so clear, but R_G corresponds to a correlation length.

R_G can be calculated from the slope of ln I(s) vs. s^2 plot (Guinier plot). Figure 6-1 shows typical examples of Guinier

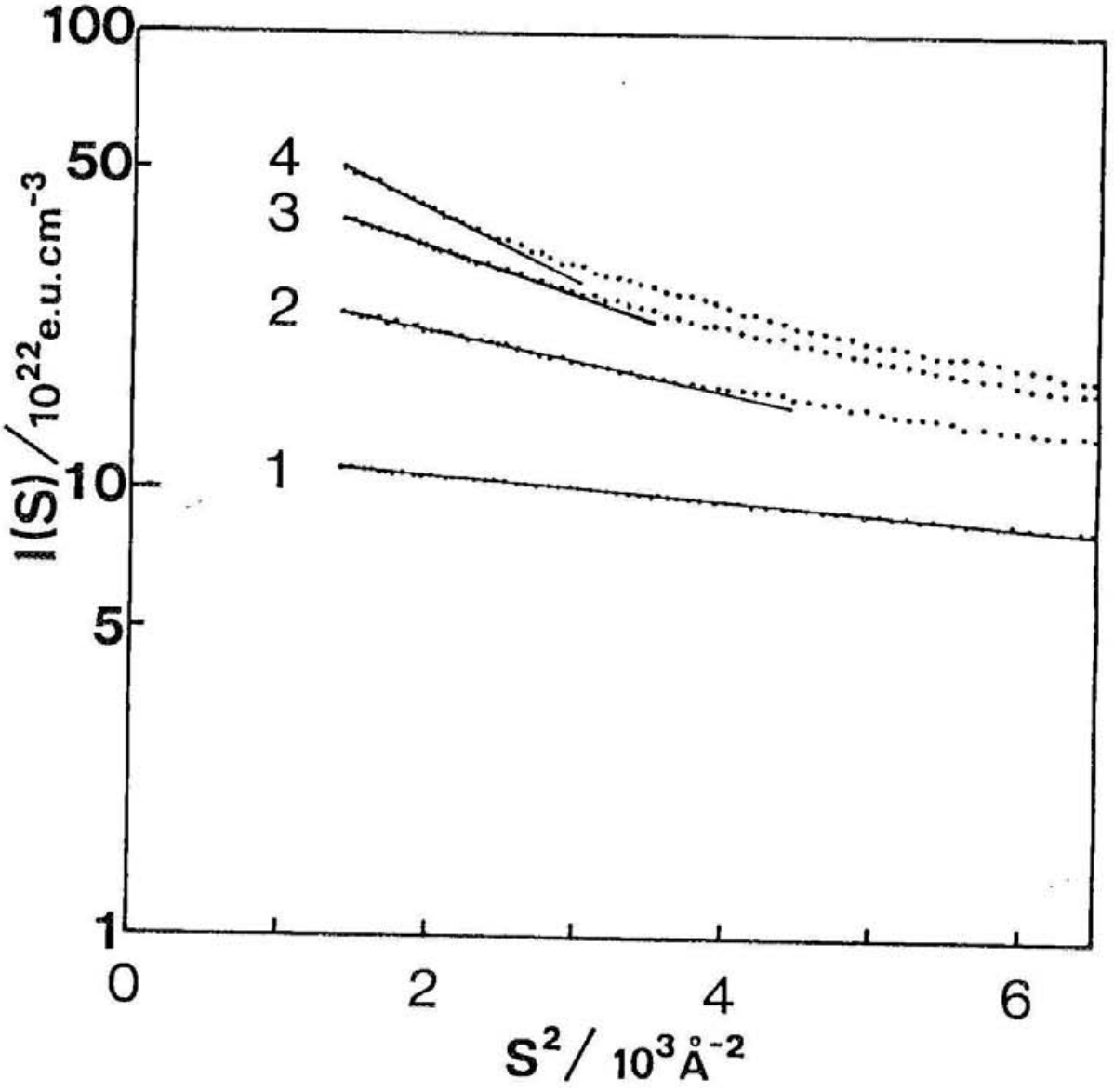

Figure 6-1. Guinier plots for NiB. The t/t_g is 1)0.24, 2)0.45, 3)0.67, and 4)0.92. The R_G values are obtained from the slope of the straight lines.

plots for NiB, and R_G values thus obtained in each sample are plotted against normalized time t/t_g in Fig. 6-2. Figure 6-2 shows that R_G increases with time, suggesting that the cluster size increases as expected.

In the region $sR_G >> 1$, the I(s) depends on the geometric structure of the scatterer and follows the Porod law as follows:[4,6,7]

$$I(s) \propto s^{-\mu}, \tag{6-3}$$

where μ is called the Porod slope.[8] When μ is less than or equal to 3, μ can be related to the mass fractal dimension of the scatter (D): $\mu = D$.[4,6]

μ can be obtained from the slope of the double logarithmic plot of I(s) vs. s (Porod plot). Figure 6-3 shows typical examples of Porod plots for NiB, and the μ values obtained for each sample are plotted against t/t_g in Fig. 6-4. The μ values in the final stage are listed in Table 6-1.

For each sample, μ increases with time in the early stage of gelation, indicating an apparent fractal geometry change. Then μ reaches constant, which shows that the geometric structure in a relatively short scale ($< d_{max} = 165$ Å) remains unchanged while the gelation is still in progress. The result suggests that the gelation in the later stage proceeds by coagulation of small clusters generated in the early stage.

A SAXS study has been made on the polymerization of TEOS

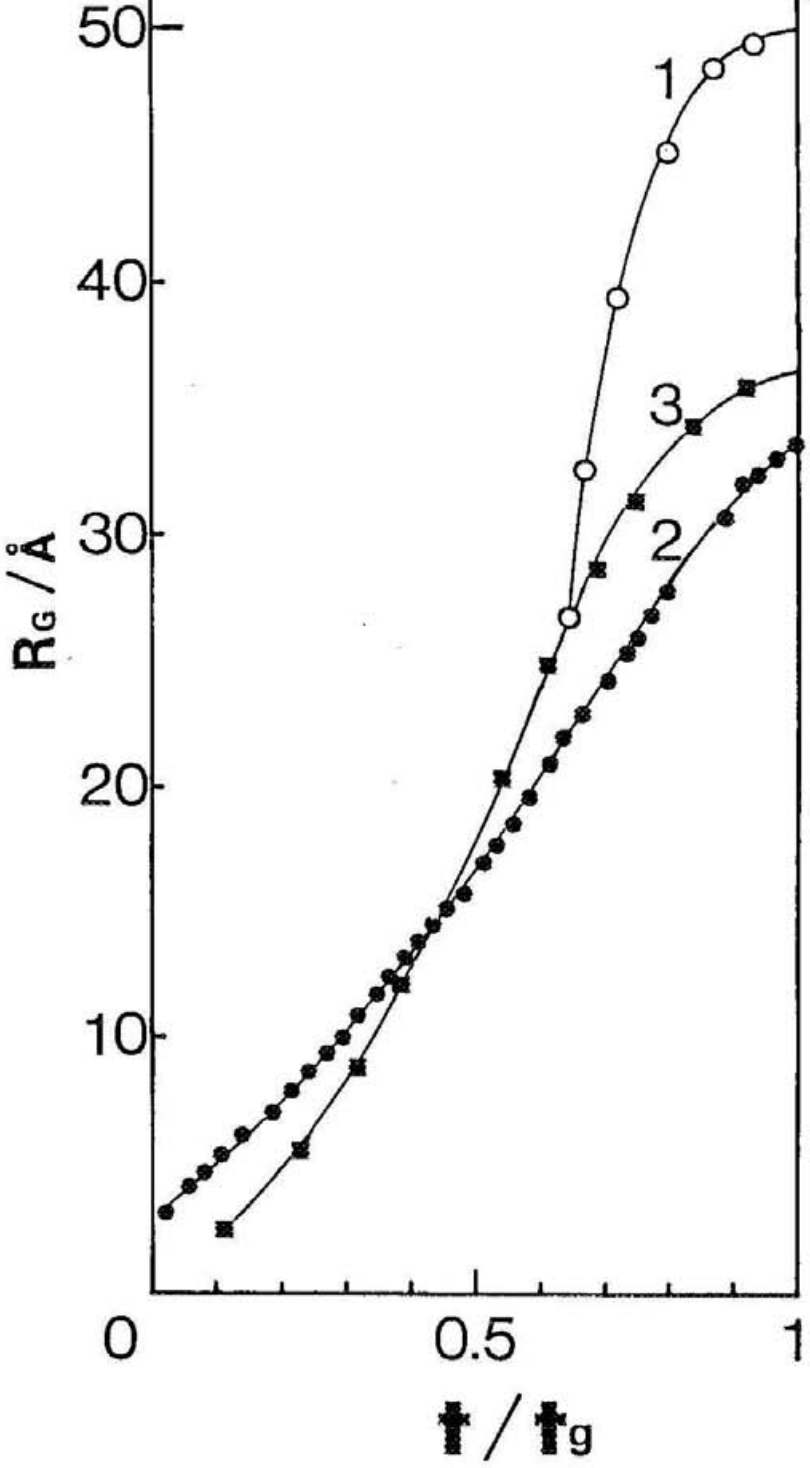

Figure 6-2. R_G values plotted against t/t_g: 1) NiA, 2) NiB, and 3) FeA.

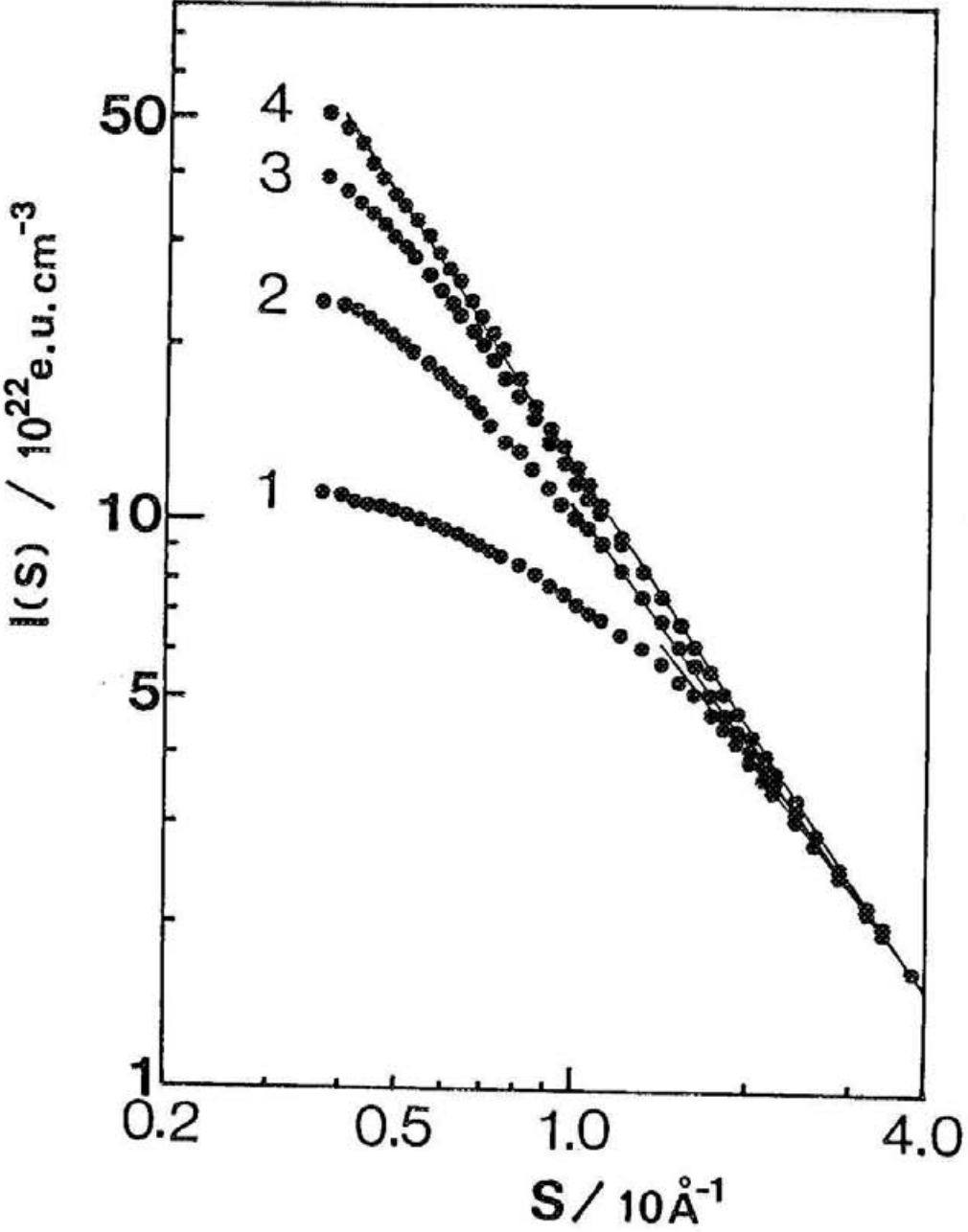

Figure 6-3. Porod plots for several data of NiB. The t/t_g is 1)0.24, 2)0.45, 3)0.67, and 4)0.92. The μ values are obtained from the slope of the straight lines.

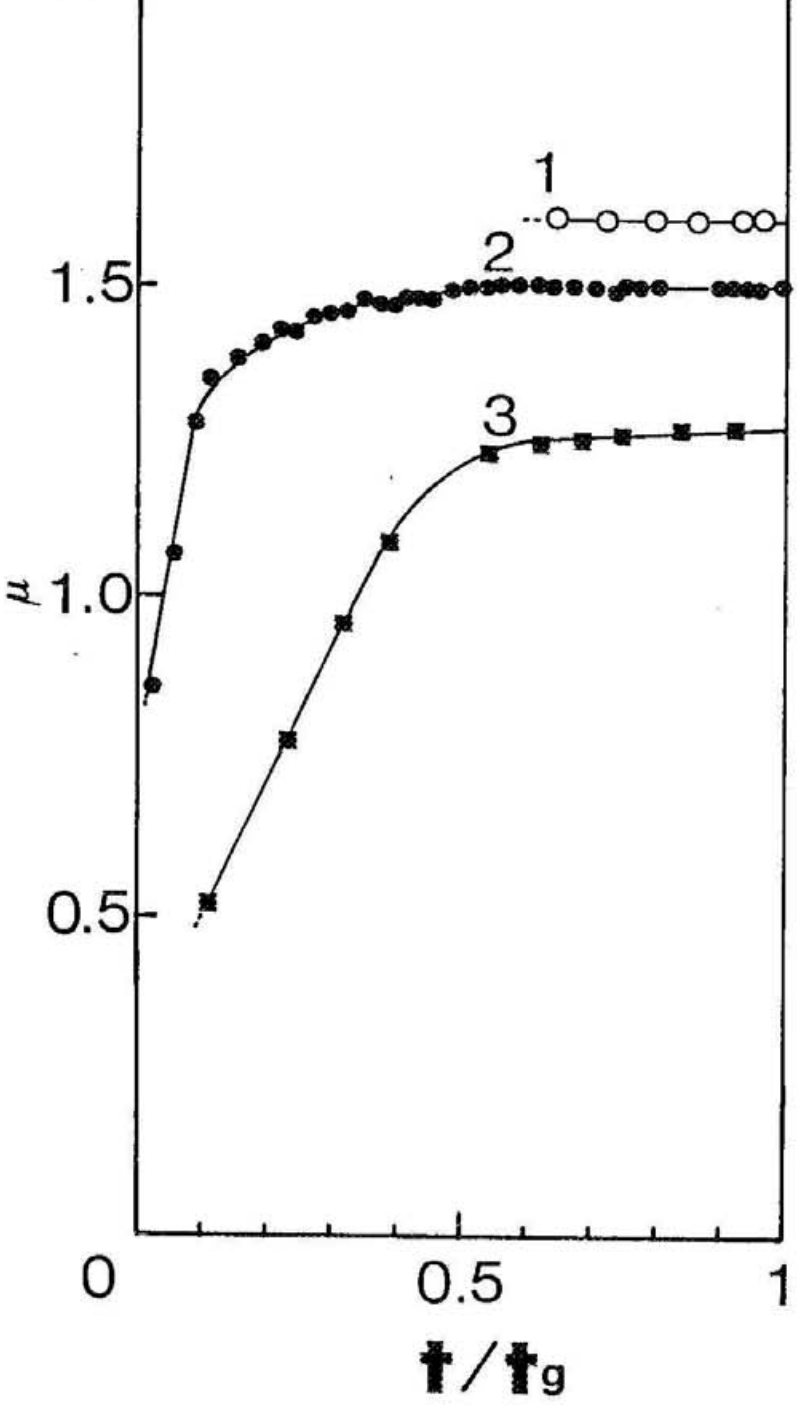

Figure 6-4. μ values plotted against t/t_g: 1) NiA, 2) NiB, and 3) FeA.

Table 6-1. μ values of metal silicate clusters in the final stage.

sample	Porod slope μ
NiA	1.61
NiB	1.50
FeA	1.27

over a wide pH range (0.8 - 8.2) by Schaefer and Keefer,[6] and μ has been reported to be 2 $\pm$ 0.1, irrespective of pH or the extent of reaction. Out of several fractal models which are consistent with the value, they regarded the lattice animal[9] as the most likely model for the polymer. Since the lattice animal is the randomly branched analog of self-avoiding linear chains, it is compatible with the chemical intuition that growth of the tetrahedral O-Si-O network takes place during the polymerization reaction.

In this study μ values observed are somewhat smaller than 2, indicating the structure of the gels containing metals is different from that made of pure TEOS and water. Several reasons can be conceived; the inclusion of metal atoms expressed by eq. (6-1) partly truncates the growth of the tetrahedral network, or metal alkoxides has a tendency to polymerize with each other. No matter what is the reason, the difference of the gel structure is reflected to μ.

Ueno, et al.[2,3,10] observed that catalysts with small metal clusters with a uniform size distribution can be prepared by the alkoxide method and attributed it to homogeneous dispersion of metal atoms in the precursor gel. It depends, however, on several factors, such as metal species employed and the concentration of metal ions. For example, in the case of 10 wt% Fe, the average size of metal particles in the catalyst was 183 Å with large distribution,[10] whereas, it was 60 - 70 Å with much small distribution in the case of 9.2 wt% Ni.[11] Thus, metal

atoms are expected to be distributed more homogeneously in the case of Ni than Fe. It is enticing to try to correlate μ values with homogeneity of the gels. A further work should be done, however, to substantiate this consideration.

6.4 Conclusions

Growth of metal silicate clusters in mixed solutions of nickel and iron ethylene glycolates, water, and tetraethoxysilane has been observed through changes of SAXS intensity curves with time. As the polymerization proceeds, the Guinier radius increases. At an early stage of the polymerization, the fractal dimension or the Porod slope also increases, and then reaches constant, while the reaction is still in progress. A relation between the fractal dimension and the properties of the gel has been discussed.

References

1. T. Uchijima, J. M. Herrman, Y. Inoue, R. L. Burwell, J. B. Buff, and J. B. Cohen, J. Catal., **50**, 464 (1977).
2. A. Ueno, H. Suzuki, and Y. Kotera, J. Chem. Soc. Faraday Trans., **79**, 127 (1983).
3. K. Tohji, Y. Udagawa, S. Tanabe, and A. Ueno, J. Am. Chem. Soc., **106**, 612 (1984).
4. D. W. Schaefer, Science, **243**, 1023 (1989).
5. A. Guinier and G. Fournet, "Small-Angle Scattering of X-Rays," Wiley, New York (1955), Ch. 2.
6. D. W. Schaefer and K. D. Keefer, Phys. Rev. Lett., **53**, 1383 (1984).
7. Y. Izumi, Phys. Rev., A **39**, 5826 (1989).
8. G. Porod, "Small Angle X-Ray Scattering," ed. O. Glatter and O. Kratky, Academic Press, London (1982), Ch. 2.
9. D. Stauffer, "Introduction to Percolation Theory," Taylor & Francis, London (1985), ch. 2.
10. S. Tanabe, T. Ida, M. Suginaga, A. Ueno, Y. Kotera, K. Tohji, and Y. Udagawa, Chem. Lett., (1984) 1567.
11. H. Suzuki, S. Takasaki, F. Koga, A. Ueno, Y. Kotera, T. Sato, and N. Todo, Chem. Lett., (1982) 127.

Acknowledgements

The author would like to express his sincerest appreciation to Professor Yasuo Udagawa (Research Institute for Scientific Measurements, Tohoku University) for his helpful guidance and encouragement throughout the course of this work.

The author is heartily grateful to Professor Kazuyuki Tohji (Tohoku University) for his valuable discussion and supports for this work.

The author deeply acknowledges Professor Hitoshi Ohtaki (the Graduate University for Advanced Studies) for his help in the preparation of this thesis.

The author is greatly indebted to Messrs. Toshio Horigome, Kouichi Suzui, Norio Okada, Nobuo Mizutani, and Shinji Kato of the machine shop of Institute for Molecular Science for their help in the construction of the SAXS diffractometer.

The author deeply acknowledges Professor Keiko Nishikawa (Yokohama National University) for her beneficial comment and encouragement in the SAXS study of NPA aqueous solutions.

The author would like to thank Professor Akifumi Ueno and Dr. Takanori Mizushima (Toyohashi University of Technology) for their assistance in the study of the growth of metal silicate.

Finally, the author wishes to acknowledge the staffs of the Graduate University for Advanced Studies who provide excellent circumstances for the research work.

List of Publications

1. H. Hayashi, K. Tohji, and Y. Udagawa,
"Construction of a Point-Focusing Small-Angle X-Ray Scattering Diffractometer for the Study of Fluctuations in Solutions",
Jpn. J. Appl. Phys., **30**, 870 (1991).

2. H. Hayashi and Y. Udagawa,
"Mixing State of 1-Propanol Aqueous Solutions Studied by Small-Angle X-Ray Scattering: A New Parameter Reflecting the Shape of SAXS Curve",
Bull. Chem. Soc. Jpn., **65**, 155 (1992).

3. H. Hayashi and Y. Udagawa,
"SAXS Curve Shape Analysis of 2-Butoxyethanol Aqueous Solutions",
Bull. Chem. Soc. Jpn., **65**, 600 (1992).

References

1. K. Nishikawa, H. Hayashi, and T. Iijima,
"Temperature Dependence of the Concentration Fluctuation, the Kirkwood-Buff Parameters, and the Correlation Length of tert-Butyl Alcohol and Water Mixtures Studied by Small-Angle X-ray Scattering",
J. Phys. Chem., **93**, 6559 (1989).

2. H. Hayashi, K. Nishikawa, and T. Iijima,
"Construction of a Small-Angle X-Ray Scattering Diffractometer for the Study of Fluctuations in Solutions",
Jpn. J. Appl. Phys., **28**, 1501 (1989).

3. H. Hayashi, K. Nishikawa, and T. Iijima,
"Small-Angle X-ray Scattering Study of Fluctuations in 1-Propanol-Water and 2-Propanol-Water Systems",
J. Phys. Chem., **94**, 8334 (1990).

4. H. Hayashi, K. Nishikawa, and T. Iijima,
"Easy Derivation of the Formula Relating the Fluctuations of a Binary System to the X-ray Scattering Intensity Extrapolated to s=0",
J. Appl. Cryst., **23**, 134 (1990).